High performance computer simulations of the subsurface radar location of celestial bodies.

Yaroslaw A. ILYUSHIN

Moscow State University
Russia Moscow 119992 GSP-2 Lengory phone +7 (495) 939-3252
e-mail ilyushin@phys.msu.ru

Institute of Radio-engineering and Electronics ulitza Mokhovaya, 11/7
125009 Moscow Russia phone 007 (495) 629-35-74

What is beneath?

Searching for the subsurface water

Earlier

Nowadays

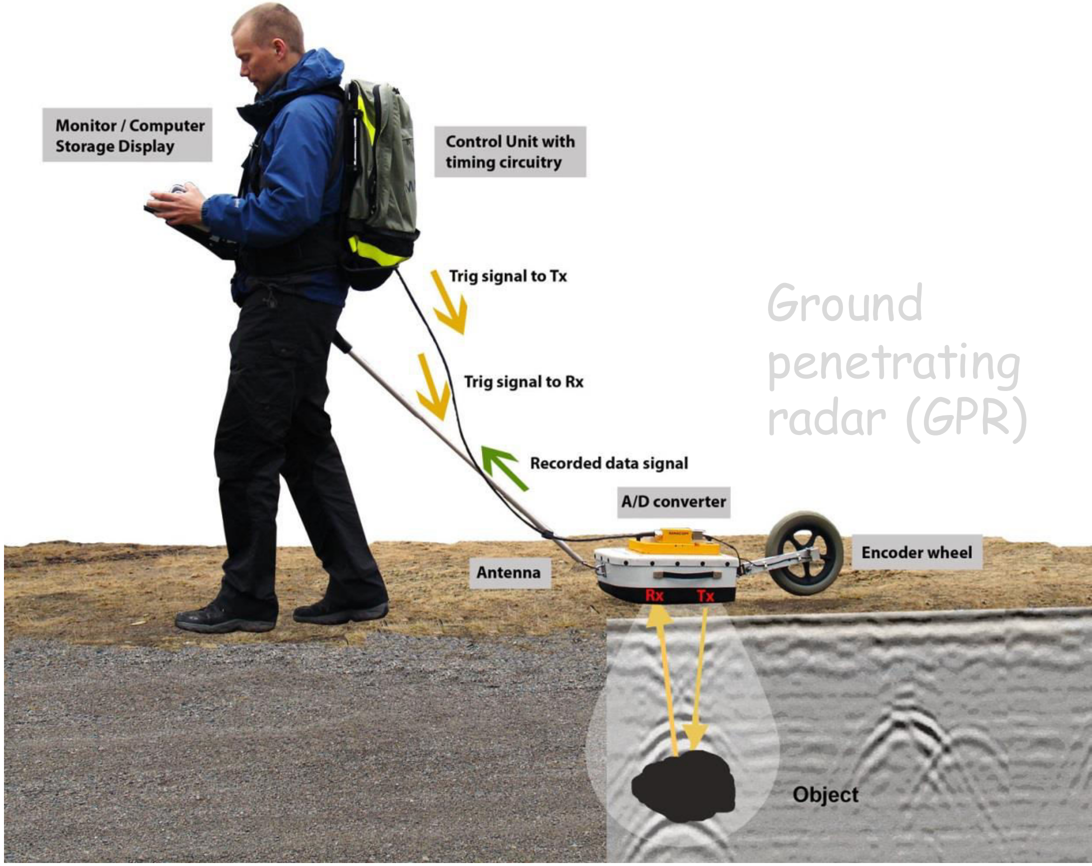

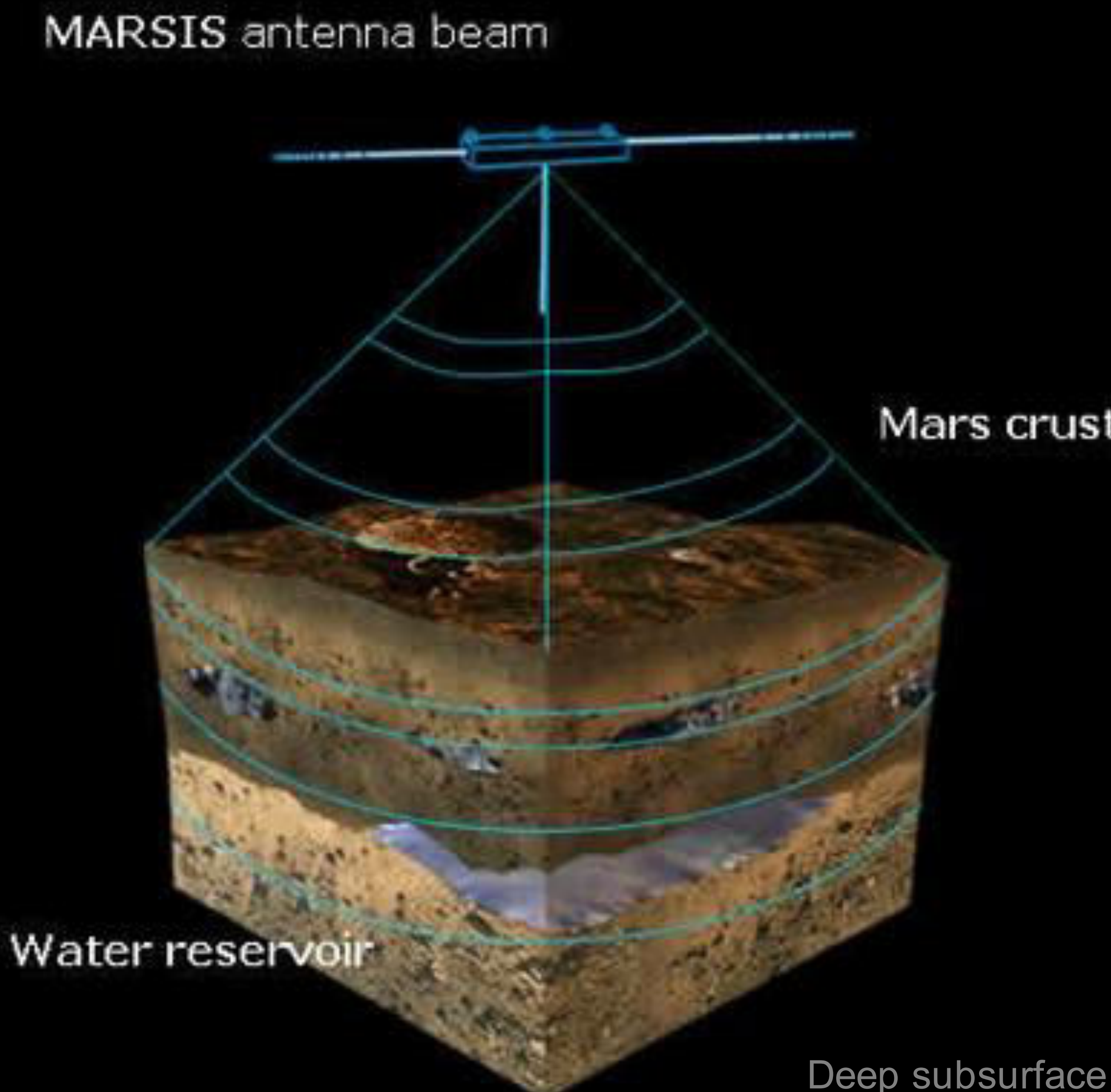

Deep subsurface sounding

GPR space instruments: the historical review

ALSE (Apollo 17, Moon)
MARSIS (Mars, Mars Express)
SHARAD (Mars, Mars Reconnaissance Orbiter)
LRS (Moon, Kaguya)

CONSERT radio wave sounder (ROSETTA, 67/P)

Planned now:
RIME (Jovian icy moons, JUICE)
REASON (Jovian icy moons)

Techniques of radar sounding of the Solar system celestial bodies

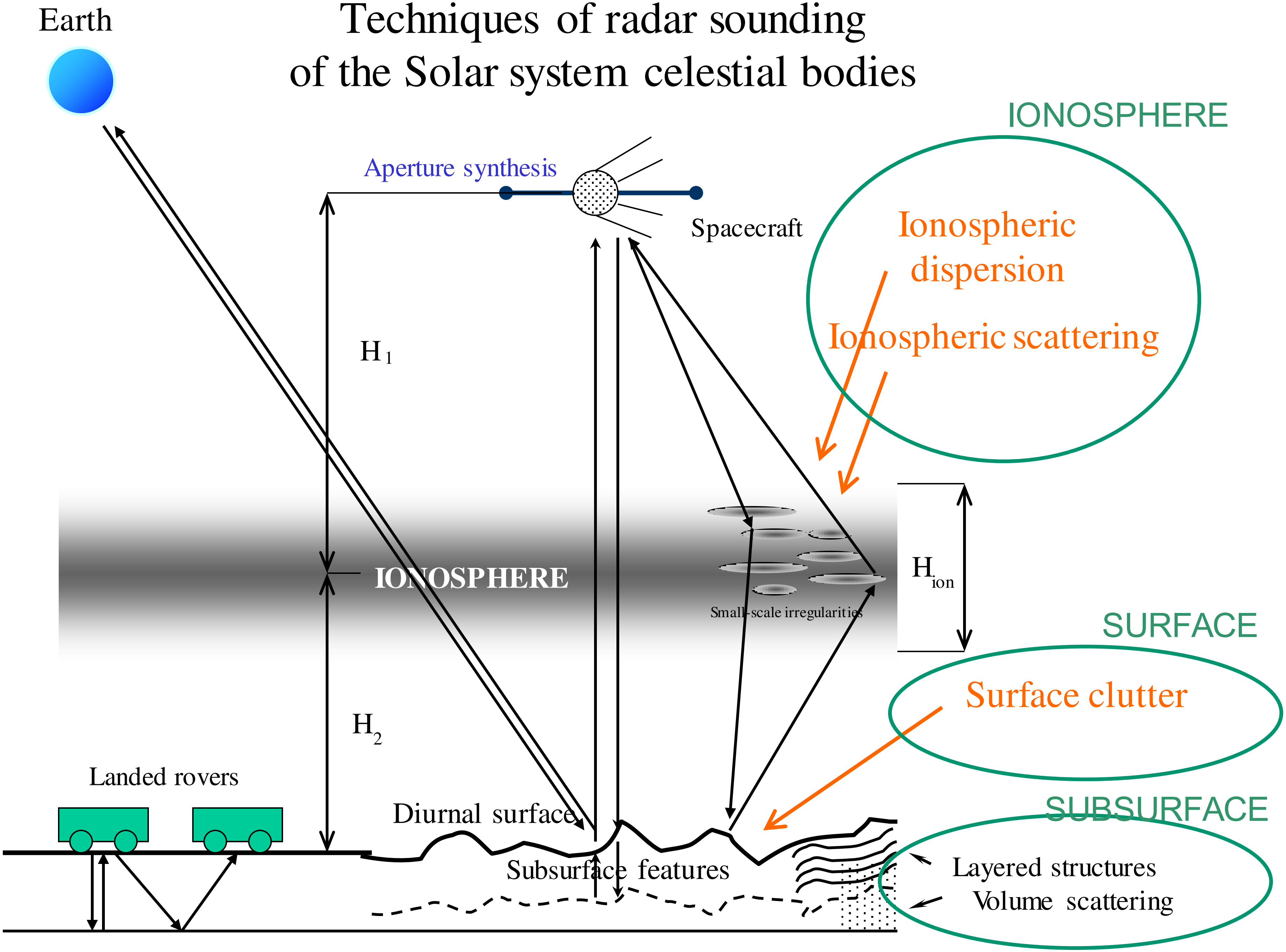

UWB LFM signal processing

Compressed signal after matched filtration

$$s(t)=\frac{1}{2\pi}\int_{-\infty}^{+\infty}F^{*}(\omega)F(\omega)H(\omega)\exp\left(-i\omega t+\varphi(\omega)-\tilde{\varphi}(\omega)\right)d\omega$$

$$\varphi(\omega)=2k\int_{0}^{z}n(z)dz$$ - systematic ionospheric phase shift

$$\tilde{\varphi}(\omega)$$ - phase correcting function

$$\omega=2\pi f\;\; n(z)=\sqrt{1-\frac{\omega_p^2(z)}{\omega^2}}\;,\; \omega_p^2=3392N[m^{-3}],\; k=\frac{\omega}{}\;.$$

Two-frequency correlation function

$$H(\omega)$$ - spectral window function (Hanning)

Amplitude mean square (mean power) of the compressed UWB LFM signal

$$|s(t)|^2=\frac{1}{2\pi}\int_{-\infty}^{+\infty}|F(\omega_1)|^2|F(\omega_2)|^2H(\omega_1)H(\omega_2)\Gamma(\omega_1,\omega_2)$$

$$\exp\left(-i(\omega_1-\omega_2)t+(\varphi(\omega_1)-\tilde{\varphi}(\omega_1))-(\varphi(\omega_2)-\tilde{\varphi}(\omega_2))\right)d\omega_1 d\omega_2$$

Surface Clutter
(Side Reflections Coming From the Rough Surface)

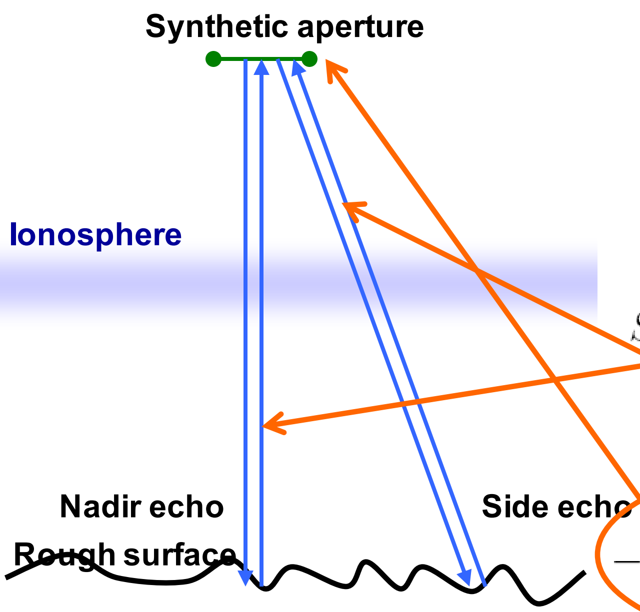

Two frequency correlation function

$$\Gamma_{\omega_1\omega_2} = \langle E_{\omega_1} E^*_{\omega_2} \rangle = \frac{e^{2i(k_1-k_2)z}}{z\pi L_1 L_2} \frac{k_1 k_2}{4\pi^2 z^2} \int e^S dx_2 dy_2 dx_5 dy_5 dl_1 dl_2$$

Propagation

$$S = \frac{ik_1}{2z}(x_1-x_2)^2 + \frac{ik_1}{2z}(y_1-y_2)^2 + \frac{ik_1}{2z}(x_2-x_3)^2 + \frac{ik_1}{2z}(y_2-y_3)^2$$
$$-\frac{ik_2}{2z}(x_1-x_5)^2 - \frac{ik_2}{2z}(y_1-y_5)^2 - \frac{ik_2}{2z}(x_5-x_3)^2 - \frac{ik_2}{2z}(y_5-y_3)^2$$
$$-\frac{(l_1-l_{01})^2}{L_1^2} - \frac{(l_2-l_{02})^2}{L_2^2} - 2(k_1^2+k_2^2) < h^2 > +\beta\rho(x_2-x_5, y_2-y_5)$$

Rough surface

Aperture synthesis

where $\beta = 4k_1k_2 < h^2 >$

Gaussian height correlation function

$$\rho(\delta\vec{r}) = \langle h(\vec{r}) h(\vec{r}+\delta\vec{r}) \rangle = \langle h^2 \rangle \exp\left(-\frac{\delta x^2}{\sigma_x^2} - \frac{\delta y^2}{\sigma_y^2}\right)$$

Exponential height correlation function

$$\rho(\delta\vec{r}) = \langle h(\vec{r}) h(\vec{r}+\delta\vec{r}) \rangle = \langle h^2 \rangle \exp\left(-\left|\frac{\delta x}{r_0}\right|\right)$$

Side clutter.
Two frequency correlation function evaluation

$$\int \exp\left(-A_{ij}x_i x_j + B_i x_i + C\right) d^n x = \sqrt{\frac{\pi^n}{det A_{ij}}} \exp\left(\frac{B^T A_{ij}^{-1} B}{4} + C\right)$$

$$A_{ij} = \begin{pmatrix} \frac{n}{\sigma_x^2} - \frac{ik_1}{z} & 0 & -\frac{n}{\sigma_x^2} & 0 & \frac{ik_1 \cos\phi}{z} & 0 \\ 0 & \frac{n}{\sigma_y^2} - \frac{ik_1}{z} & 0 & -\frac{n}{\sigma_y^2} & \frac{ik_1 \sin\phi}{z} & 0 \\ -\frac{n}{\sigma_x^2} & 0 & \frac{ik_2}{z} + \frac{n}{\sigma_x^2} & 0 & 0 & -\frac{ik_2 \cos\phi}{z} \\ 0 & -\frac{n}{\sigma_y^2} & 0 & \frac{ik_2}{z} + \frac{n}{\sigma_y^2} & 0 & -\frac{ik_2 \sin\phi}{z} \\ \frac{ik_1 \cos\phi}{z} & \frac{ik_1 \sin\phi}{z} & 0 & 0 & \frac{1}{L_1^2} - \frac{ik_1}{z} & 0 \\ 0 & 0 & -\frac{ik_2 \cos\phi}{z} & -\frac{ik_2 \sin\phi}{z} & 0 & \frac{ik_2}{z} + \frac{1}{L_2^2} \end{pmatrix}$$

$$B_i = \left\{-\frac{i\delta l_1 k_1 \cos\phi}{z}, -\frac{i\delta l_1 k_1 \sin\phi}{z}, \frac{i\delta l_2 k_2 \cos\phi}{z}, \frac{i\delta l_2 k_2 \sin\phi}{z}, \frac{i\delta l_1 k_1}{z} + \frac{2l_0}{L_1^2}, -\frac{i\delta l_2 k_2}{z}\right\}$$

$$C = \frac{i\left(\delta l_1^2 k_1 - \delta l_2^2 k_2\right)}{2z} - \frac{l_0^2}{L_1^2}.$$

Side clutter.
Two frequency correlation function evaluation

$$\langle E_{\omega_1} E^*_{\omega_2} \rangle = \sum_{n=0}^{\infty} \frac{(\beta^n/n!) k_1 k_2 \sigma_x \sigma_y \exp\left(- \frac{k_1 k_2 n l_0{}^2}{\left(k_1 k_2 \left(n (L_1{}^2 + L_2{}^2\right) + \sigma_x{}^2\right) - i (k_1 - k_2) n z \right)} \right)}{\sqrt{(k_1 k_2 \sigma_y{}^2 - i(k_1 - k_2) n z)\left(k_1 k_2 \left(n (L_1{}^2 + L_2{}^2\right) + \sigma_x{}^2\right) - i(k_1 - k_2) n z)}}$$

The synthetic aperture lengths can be different at different frequencies and vary with the position of the spacecraft

Spatial displacement between synthetic aperture centers at two frequencies. For the step frequency radar (SFR) must be taken into account

Anisotropic surface roughness height correlation function

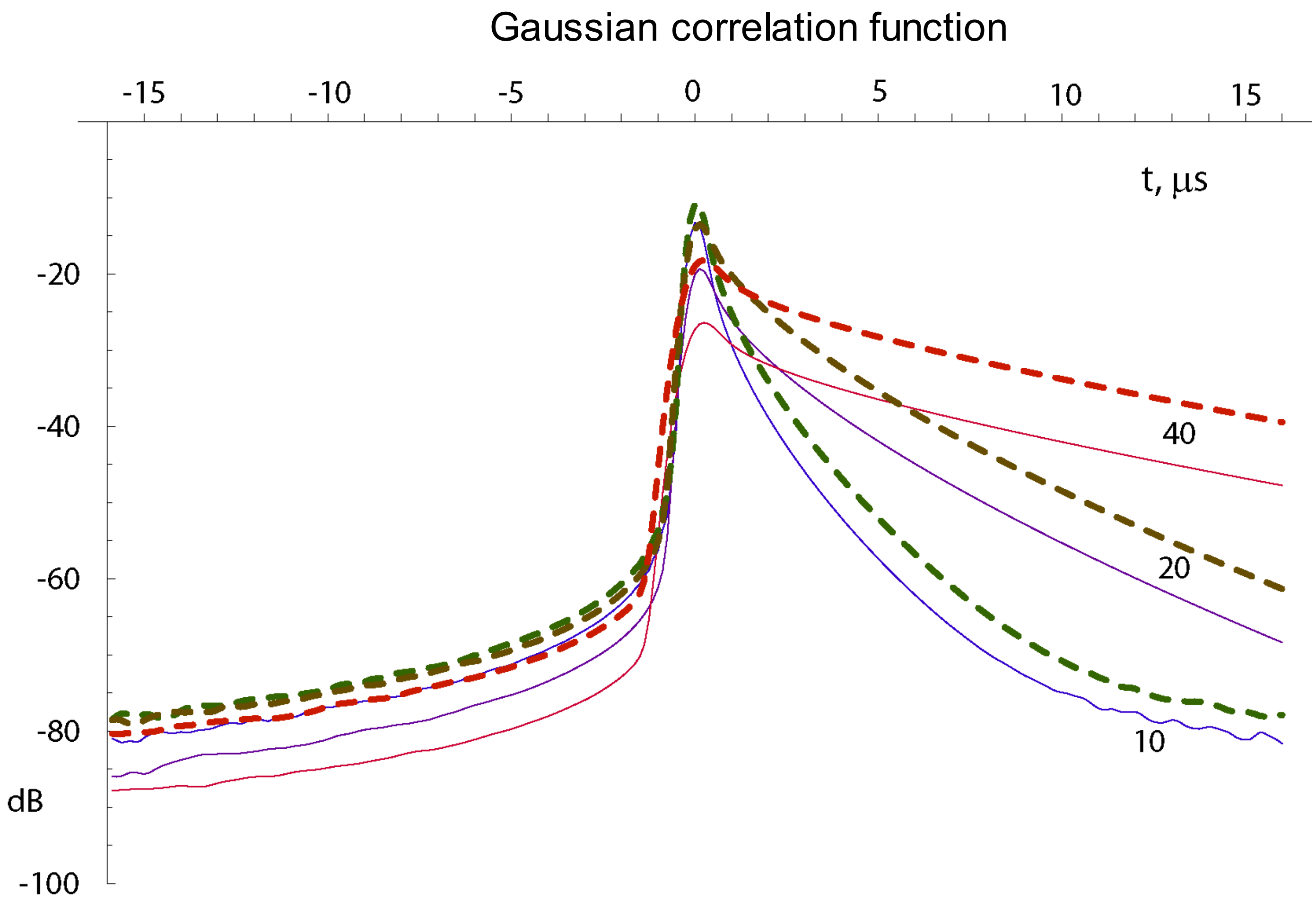

Compressed UWB LFM signals coming from rough front surface. Solid curves correspond to σ_x=1000 м, dashed curves - σ_x=10000 м. For all signals σ_y=1000 м. R.m.s. roughness height deviation shown by numbers near each curve.

Rough surface reflection from the planet: radar equation approximation

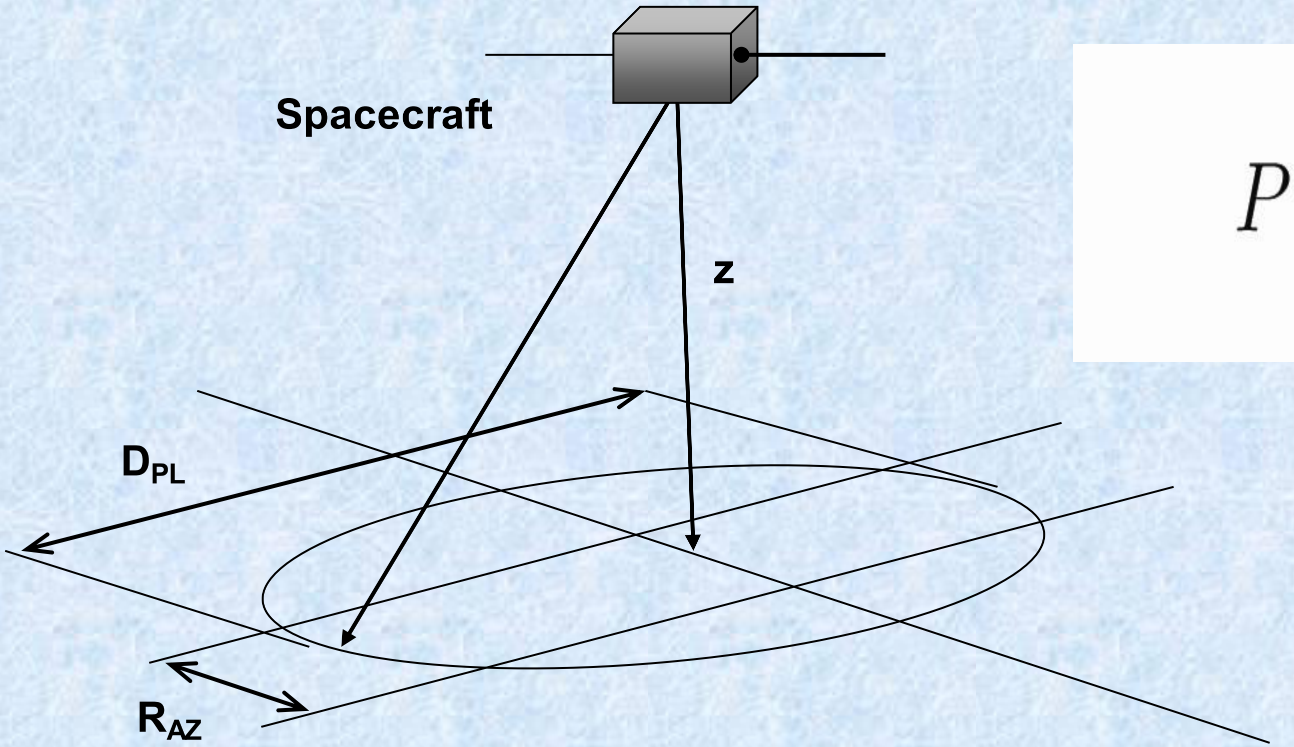

$$P = P_0 \frac{g^2 \lambda^2 \sigma_0 A}{(4\pi)^3 z^4},$$

Radar equation

$$A = R_{AZ} D_{PL}$$

Diffuse scattering area

$$D_{PL} \approx 2\sqrt{zc\tau}$$

Radar pulse length limited diameter of the scattering area

$$R_{AZ} = \lambda z / 2L_s$$

Azimuth resolution of the radar

Hagfors' law: reflection from the rough surface

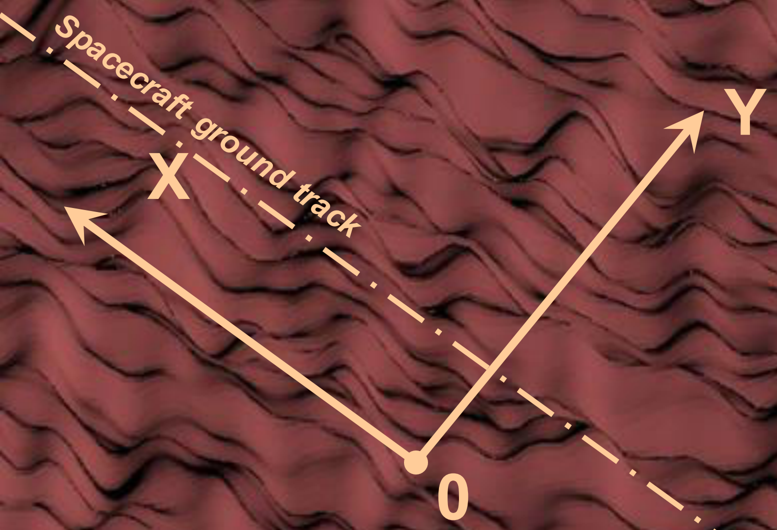

Exponential surface roughness height correlation function

$$\rho(\delta\vec{r}) = \langle h(\vec{r})h(\vec{r}+\delta\vec{r})\rangle = \langle h^2\rangle \exp\left(-\left|\frac{\delta x}{r_0}\right|\right)$$

Hagfors' roughness parameter

$$C = \frac{\lambda^2 r_0^2}{16\pi^2 \langle h^2\rangle^2}$$

Scattering cross section of the unit area

$$\sigma_H(\vartheta) = \frac{R}{2}\frac{C}{\left(\cos^4\vartheta + C\sin^2\vartheta\right)^{3/2}}$$

Normalized diffuse reflection power from the nadi

$$\frac{\sigma_0 z}{\pi z^2} = \frac{1}{2}\left(\frac{\sigma\lambda}{4\pi < h^2 >}\right)^2 \frac{\lambda z^{3/2}(c\tau)^{1/2}}{L_s}.$$

Exponential height correlation function: Hagfors' law test

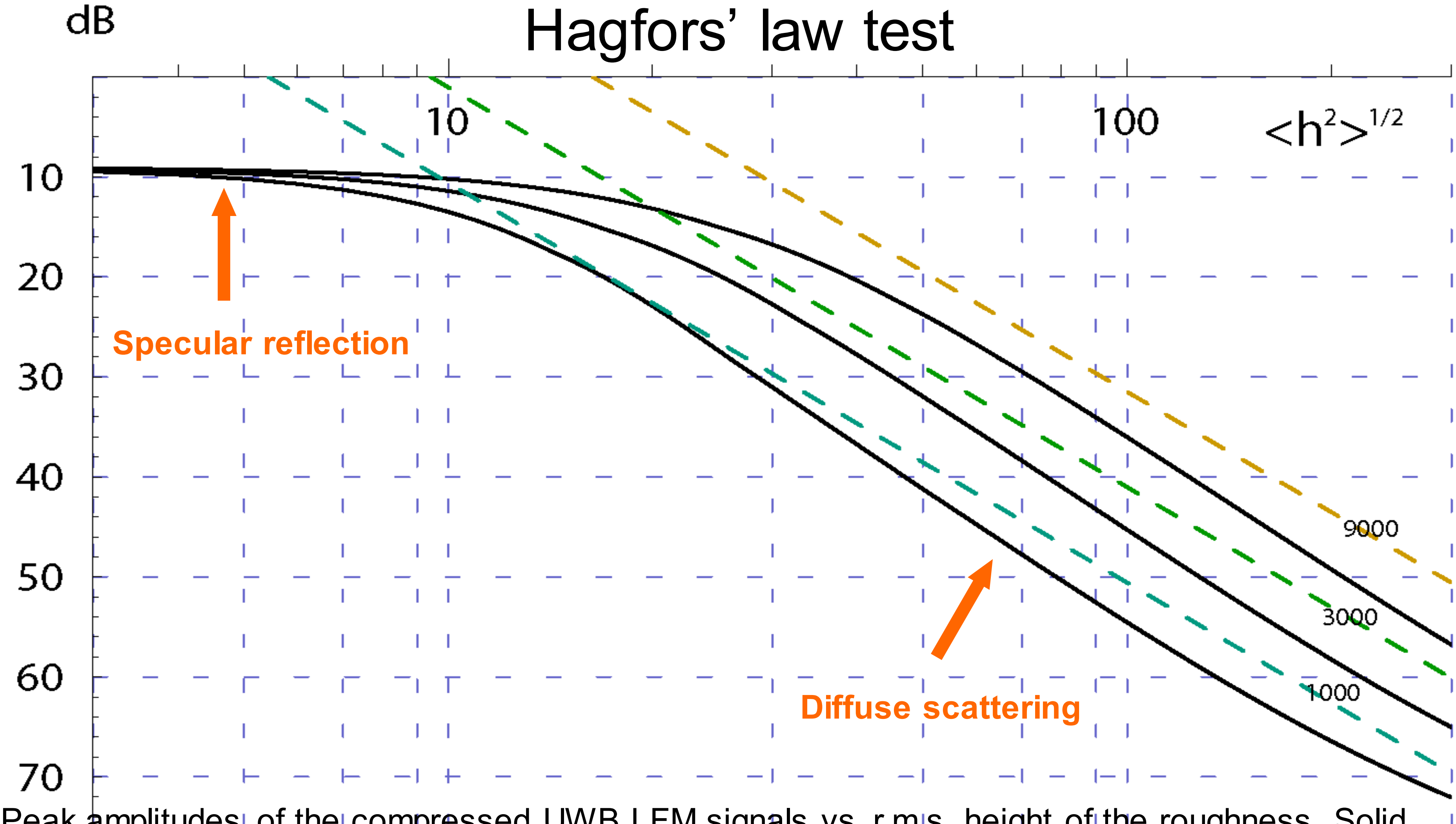

Peak amplitudes of the compressed UWB LFM signals vs. r.m.s. height of the roughness. Solid **black** curves – amplitude calculation through the two frequency correlation function, dashed **colored** curves – approximate estimation by the unit area scattering cross section (radar equation). Height correlation functions are isotropic, correlation scales are shown near each pair of the curves by numbers.

Clutter simulation algorithm

immediate evaluation of the Kirchhoff integrals

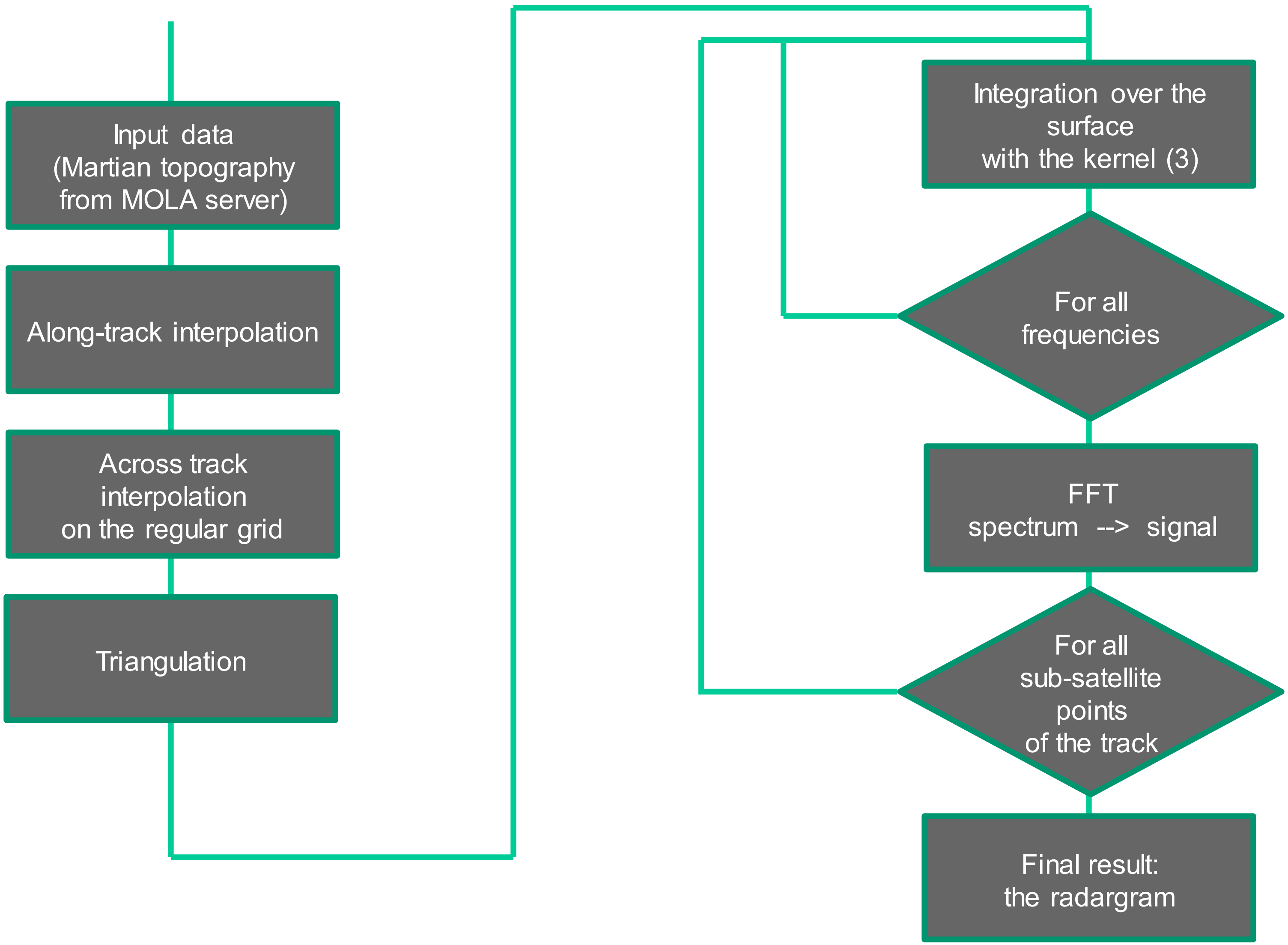

Kirchoff approximation: facet surface model (SHARSIM etc.)

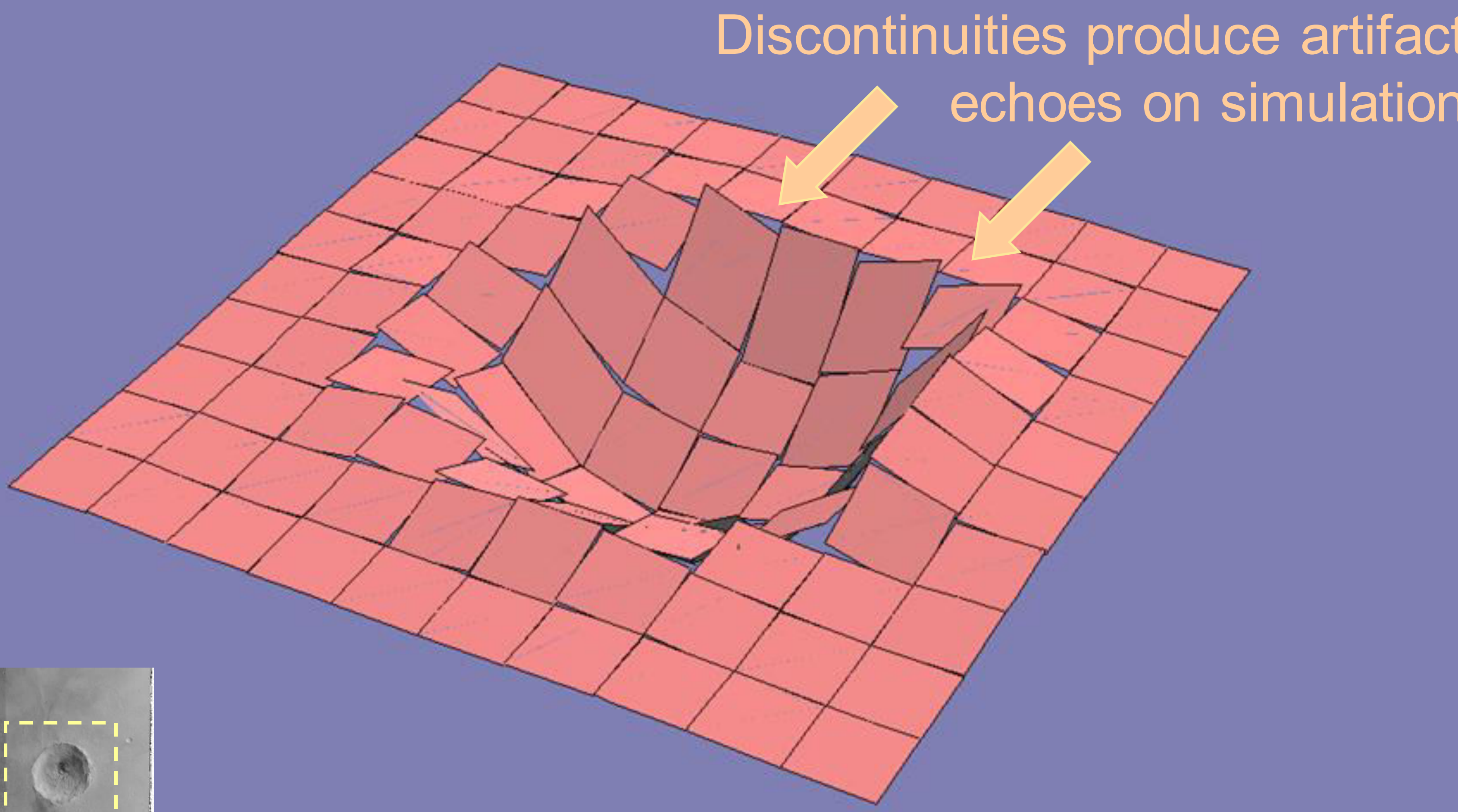

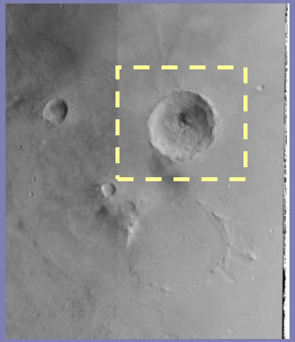

Kirchoff approximation: we use surface triangulation

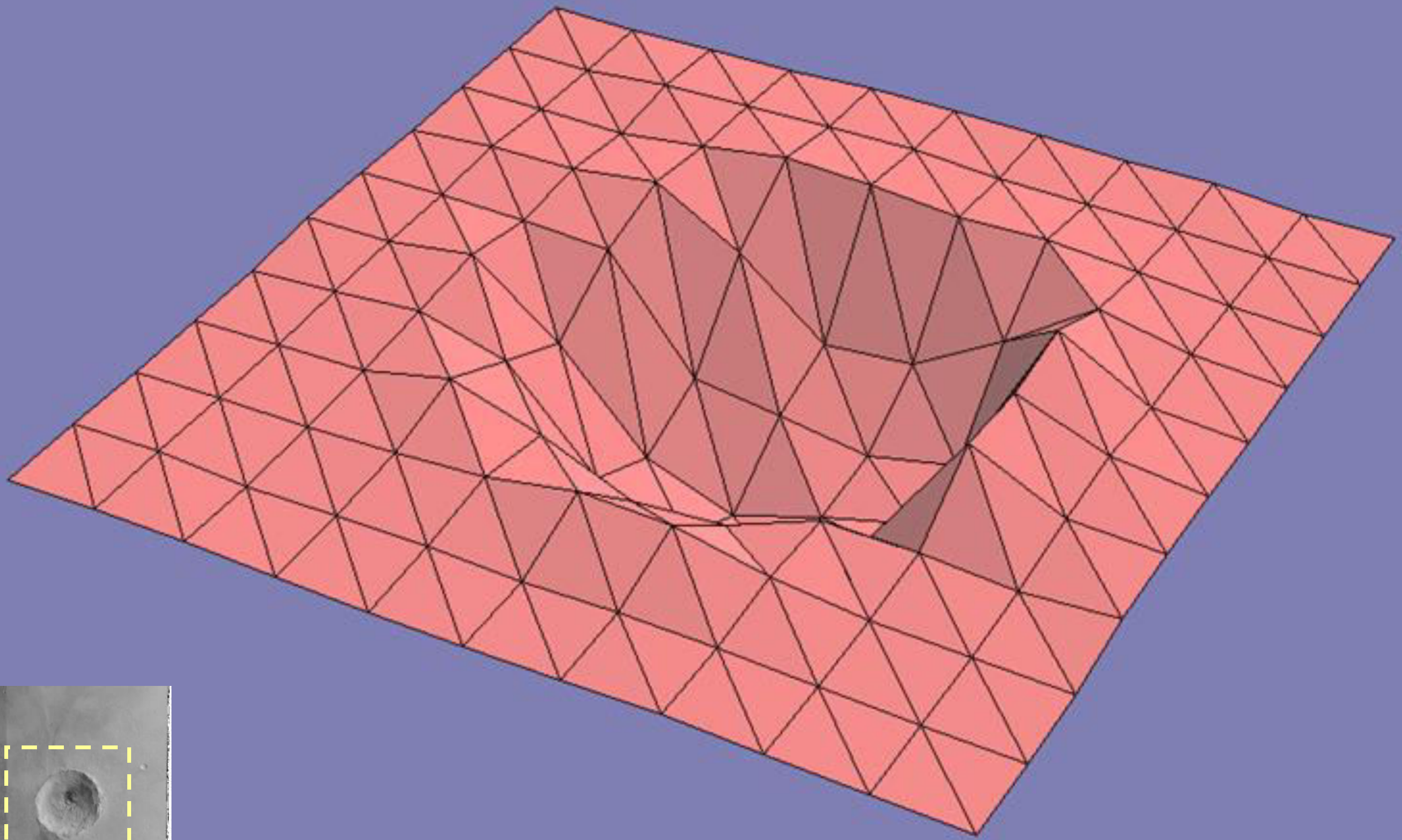

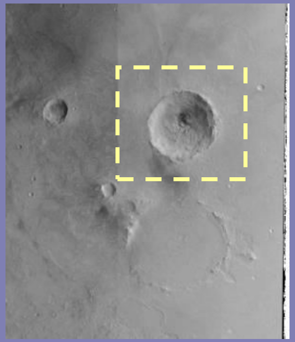

Surface is represented by a continuous function

MEX orbit 9466 (the southmost part)

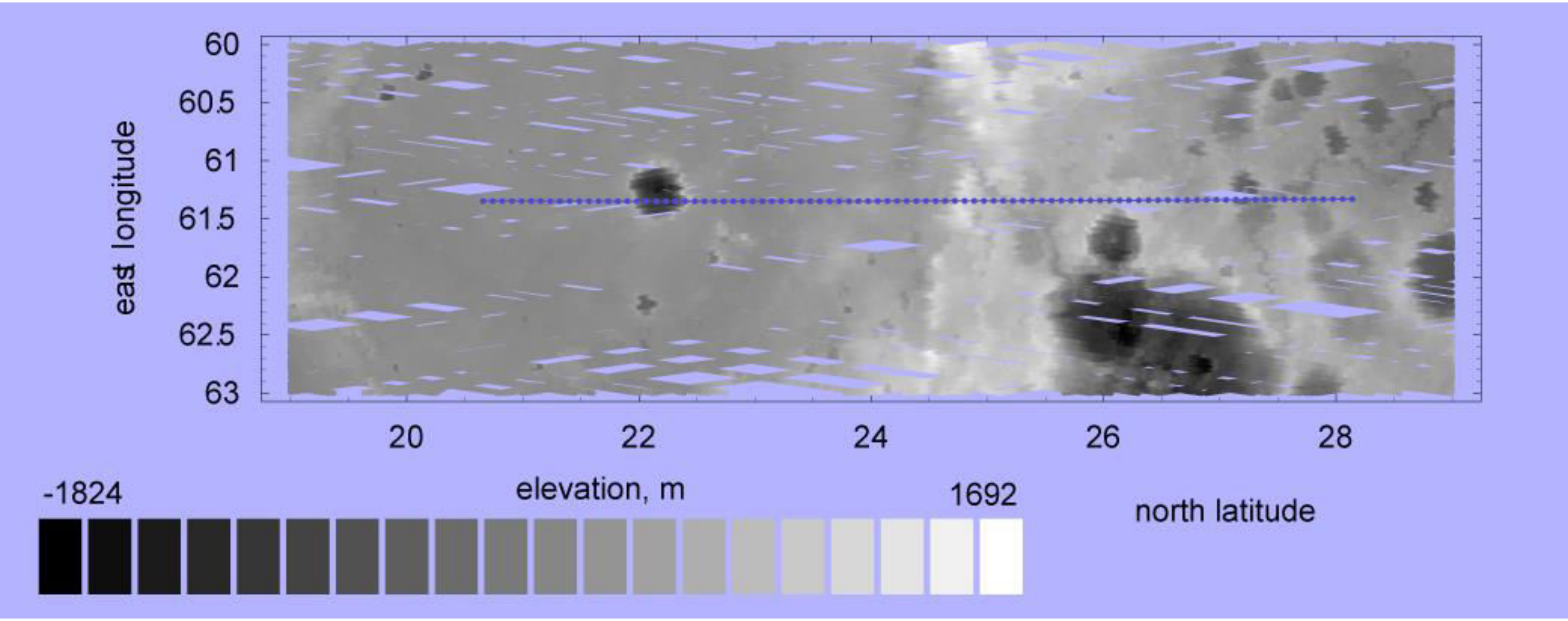

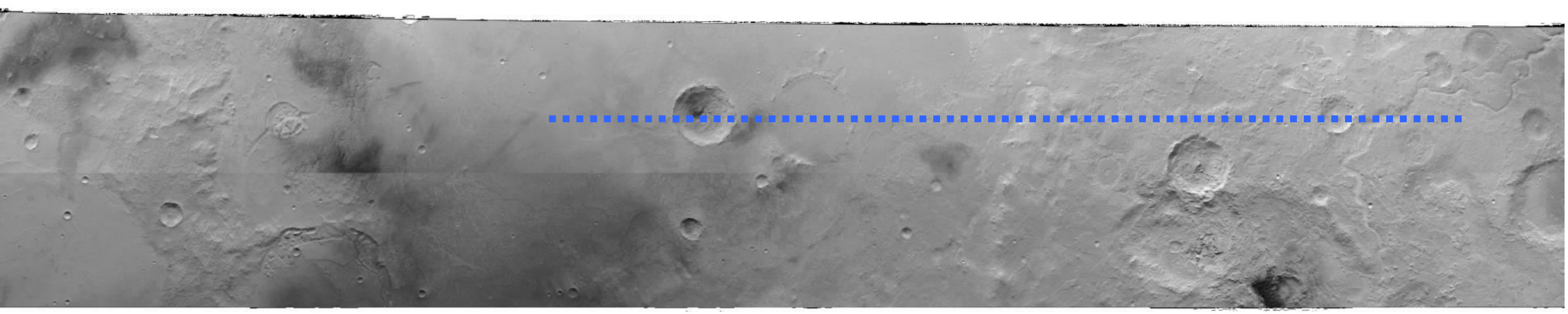

MOLA topography data (above); mosaic of HRSC images H5191_0000_ND3 and H7357_0000_ND3 (below)

MEX 9466 orbit radargrams

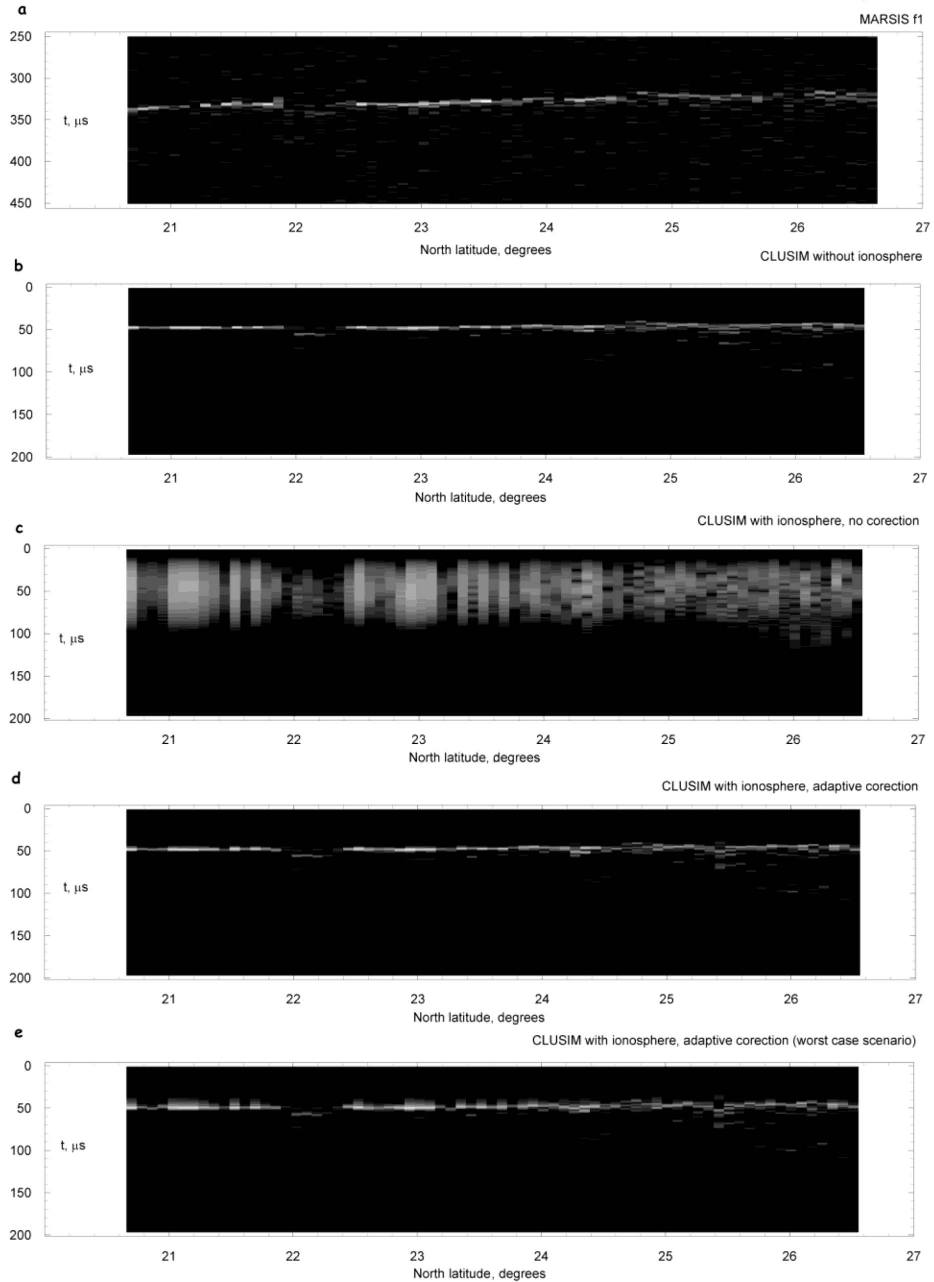

Anisotropic correlation function of the ionospheric plasma fluctuations

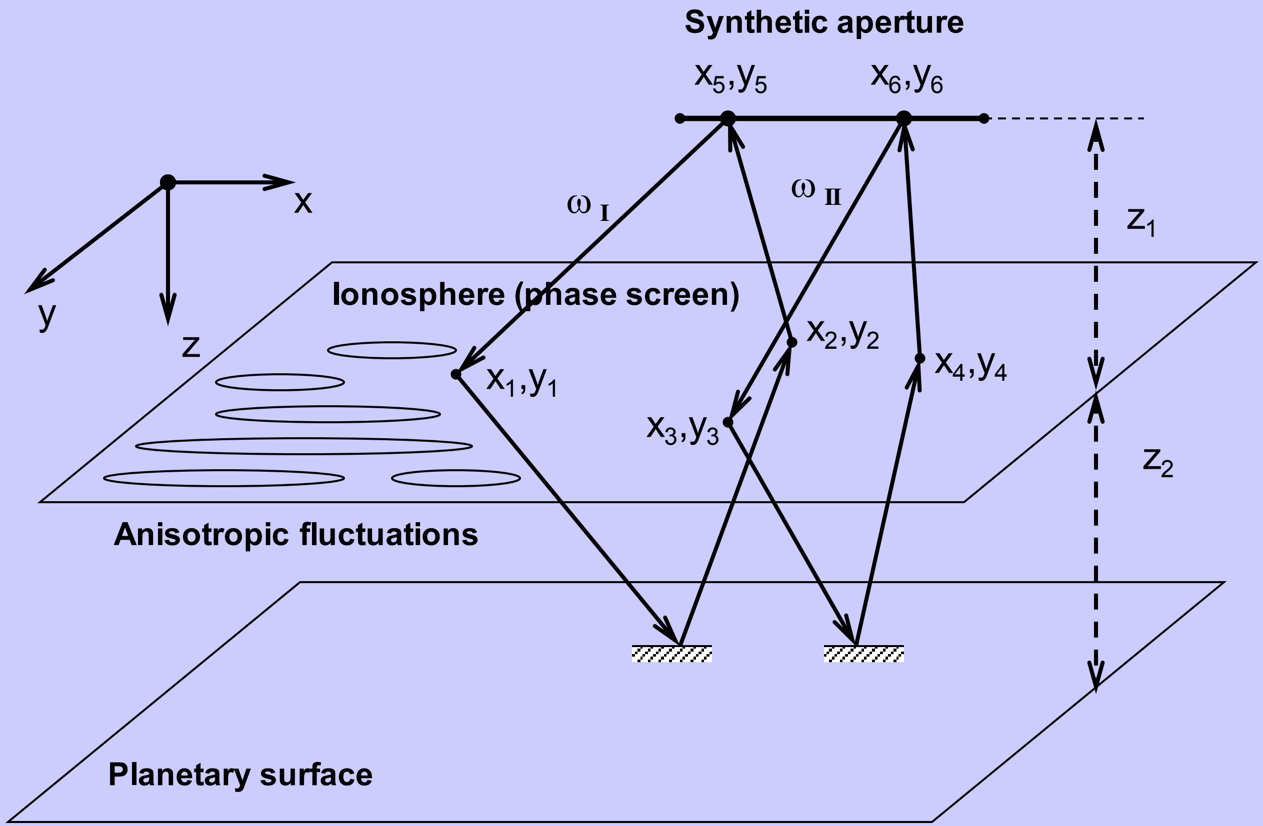

Anisotropic correlation function of the ionospheric plasma fluctuations: coherency function $\Gamma(\omega_I,\omega_{II})$

Random phases
must be averaged all together

$$
\begin{aligned}
\Gamma(\omega_I,\omega_{II}) = {} & \frac{1}{z_1^2}\frac{k_I}{2\pi i\,2z_2}\frac{k_I}{2\pi i\,z_1}\frac{1}{\sqrt{\pi}L}\frac{k_{II}}{2\pi i\,2z_2}\frac{k_{II}}{2\pi i\,z_1}\frac{1}{\sqrt{\pi}L}\int dx_1dy_1dx_2dy_2dx_5dx_3dy_3dx_4dy_4dx_6 \\
& \exp\Bigg(ik_Iz_1+\frac{ik_I(x_5-x_1)^2+ik_I(y_5-y_1)^2}{2z_1}+2ik_Iz_2+\frac{ik_I(x_1-x_2)^2+ik_I(y_1-y_2)^2}{4z_2}+i\phi(x_1,y_1) \\
& +ik_Iz_1+\frac{ik_I(x_5-x_2)^2+ik_I(y_5-y_2)^2}{2z_1}+i\phi(x_2,y_2)-\frac{(x_5-x_0)^2}{L^2}+i\frac{\pi\nu(x_5-x_0)}{L} \\
& -ik_{II}z_1-\frac{ik_{II}(x_6-x_3)^2-ik_{II}(y_5-y_3)^2}{2z_1}-2ik_{II}z_2-\frac{ik_{II}(x_3-x_4)^2-ik_{II}(y_3-y_4)^2}{4z_2}-i\phi(x_3,y_3) \\
& -ik_{II}z_1-\frac{ik_{II}(x_6-x_4)^2-ik_{II}(y_5-y_4)^2}{2z_1}-i\phi(x_4,y_4)-\frac{(x_6-x_0)^2}{L^2}-i\frac{\pi\nu(x_6-x_0)}{L}\Bigg)
\end{aligned}
$$

Synthetic aperture terms

Ionospheric phase fluctuations: effective phase screen model

Correlation function of the dielectric permittivity ε

$$B_\varepsilon(\vec{r}_1, \vec{r}_2) = < \varepsilon_1(\vec{r}_1, \omega_1)\varepsilon_1(\vec{r}_2, \omega_2) >$$

$$= \frac{\omega_{p1}^4/(\omega_1\omega_2)^2}{(1-\omega_{p0}^2/\omega_1^2)(1-\omega_{p0}^2/\omega_2^2)} \exp\left(-\frac{(x_1-x_2)^2}{\sigma_x^2} - \frac{(y_1-y_2)^2}{\sigma_y^2} - \frac{(z_1-z_2)^2}{\sigma_z^2}\right).$$

$$B_\varepsilon(\vec{\rho}, z) \approx A_{\omega_1,\omega_2}(\vec{\rho})\delta z,$$

Integrated correlation function

$$A_{\omega_1,\omega_2}(\vec{\rho}) = \int_{-\infty}^{+\infty} B_\varepsilon(\vec{\rho}, z)dz = A_{\omega_1,\omega_2}(0)\exp\left(-\frac{(x_1-x_2)^2}{\sigma_x^2} - \frac{(y_1-y_2)^2}{\sigma_y^2}\right),$$

$$A_{\omega_1,\omega_2}(0) = \frac{\omega_{p1}^4/(\omega_1\omega_2)^2}{(1-\omega_{p0}^2/\omega_1^2)(1-\omega_{p0}^2/\omega_2^2)}\sqrt{\pi}\sigma_z,$$

Random phase shift correlation coefficients

$$< \phi_i \phi_j >= \frac{H}{4} k_i k_j A_{\omega_i,\omega_j}(\vec{\rho})$$

Phase shift characteristic function
(averaged exponent of all the random phase shifts) is

$$M(\phi_1, \phi_2, \phi_3, \phi_4) = \langle \exp(i\phi_1 + i\phi_2 - i\phi_3 - i\phi_4) \rangle = \exp\left(-\frac{1}{2}\sum \lambda_{ij}\right)$$

$$M(\phi_1, \phi_2, \phi_3, \phi_4) = \sum_{\{n_{ij}\}} \prod_{i,j} \frac{\beta^{n_{ij}}}{n_{ij}!} \exp\left(-\frac{n_{ij}(x_i - x_j)^2}{\sigma_x^2} - \frac{n_{ij}(y_i - y_j)^2}{\sigma_y^2} - \frac{n_{ij}(t_i - t_j)^2}{\tau^2}\right)$$

where $\beta_{ij} = -\frac{k_i k_j H}{4} A_{\omega_i \omega_j}(0)$

(we perform the Taylor series expansion in the β_{ij})

Two frequency correlation function

$$\Gamma(\omega_I,\omega_{II}) = \left(\frac{k_I k_{II}}{z_1^2 2\pi 2 z_2}\frac{1}{\sqrt{\pi}L}\right)^2 \exp(-\beta_{22}-\beta_{44}) \sum_{\{n\}} \frac{\beta_{12}^{n_{12}}}{n_{12}!}\frac{\beta_{34}^{n_{12}}}{n_{34}!}\frac{\beta_{13}^{n_{13}}}{n_{13}!}\frac{\beta_{14}^{n_{14}}}{n_{14}!}\frac{\beta_{23}^{n_{23}}}{n_{23}!}\frac{\beta_{24}^{n_{24}}}{n_{24}!}$$

$$\int \exp\left(-A_{ij}^{(x)} x_i x_j\right) dx_1 \ldots dx_6 \int \exp\left(-A_{ij}^{(y)} y_i y_j\right) dy_1 \ldots dy_4$$

where

$$\int \exp\left(-A_{ij} x_i x_j\right) d^n x = \sqrt{\frac{\pi^n}{det A_{ij}}}$$

Matrices of the Gaussian integrals

$$A_{ij}^{(x)} = \begin{pmatrix} \frac{n_{12}+n_{13}+n_{14}}{\sigma_x{}^2} - \frac{ik_1(z_1+2z_2)}{4z_1 z_2} & \frac{ik_1}{4z_2} - \frac{n_{12}}{\sigma_x{}^2} & -\frac{n_{13}}{\sigma_x{}^2} & -\frac{n_{14}}{\sigma_x{}^2} & \frac{ik_1}{2z_1} & 0 \\ \frac{ik_1}{4z_2} - \frac{n_{12}}{\sigma_x{}^2} & \frac{n_{12}+n_{23}+n_{24}}{\sigma_x{}^2} - \frac{ik_1(z_1+2z_2)}{4z_1 z_2} & -\frac{n_{23}}{\sigma_x{}^2} & -\frac{n_{24}}{\sigma_x{}^2} & \frac{ik_1}{2z_1} & 0 \\ -\frac{n_{13}}{\sigma_x{}^2} & -\frac{n_{23}}{\sigma_x{}^2} & \frac{n_{13}+n_{23}+n_{34}}{\sigma_x{}^2} + \frac{ik_2(z_1+2z_2)}{4z_1 z_2} & -\frac{ik_2}{4z_2} - \frac{n_{34}}{\sigma_x{}^2} & 0 & -\frac{ik_2}{2z_1} \\ -\frac{n_{14}}{\sigma_x{}^2} & -\frac{n_{24}}{\sigma_x{}^2} & -\frac{ik_2}{4z_2} - \frac{n_{34}}{\sigma_x{}^2} & \frac{n_{14}+n_{24}+n_{34}}{\sigma_x^2} + \frac{ik_2(z_1+2z_2)}{4z_1 z_2} & 0 & -\frac{ik_2}{2z_1} \\ \frac{ik_1}{2z_1} & \frac{ik_1}{2z_1} & 0 & 0 & \frac{1}{L^2} - \frac{ik_1}{z_1} & 0 \\ 0 & 0 & -\frac{ik_2}{2z_1} & -\frac{ik_2}{2z_1} & 0 & \frac{ik_2}{z_1} + \frac{1}{L^2} \end{pmatrix}$$

Matrices of the Gaussian integrals

$$A_{ij}^{(y)} = \begin{pmatrix} \frac{n_{12}+n_{13}+n_{14}}{\sigma_y^2} - \frac{ik_1(z_1+2z_2)}{4z_1 z_2} & \frac{ik_1}{4z_2} - \frac{n_{12}}{{\sigma_y}^2} & -\frac{n_{13}}{{\sigma_y}^2} & -\frac{n_{14}}{{\sigma_y}^2} \\ \frac{ik_1}{4z_2} - \frac{n_{12}}{{\sigma_y}^2} & \frac{n_{12}+n_{23}+n_{24}}{\sigma_y^2} - \frac{ik_1(z_1+2z_2)}{4z_1 z_2} & -\frac{n_{23}}{{\sigma_y}^2} & -\frac{n_{24}}{{\sigma_y}^2} \\ -\frac{n_{13}}{{\sigma_y}^2} & -\frac{n_{23}}{{\sigma_y}^2} & \frac{n_{13}+n_{23}+n_{34}}{\sigma_y^2} + \frac{ik_2(z_1+2z_2)}{4z_1 z_2} & -\frac{ik_2}{4z_2} - \frac{n_{34}}{{\sigma_y}^2} \\ -\frac{n_{14}}{{\sigma_y}^2} & -\frac{n_{24}}{{\sigma_y}^2} & -\frac{ik_2}{4z_2} - \frac{n_{34}}{{\sigma_y}^2} & \frac{n_{14}+n_{24}+n_{34}}{\sigma_y^2} + \frac{ik_2(z_1+2z_2)}{4z_1 z_2} \end{pmatrix}$$

Degradation of the compressed LFM UWB signals due to anisotropic ionospheric scintillations

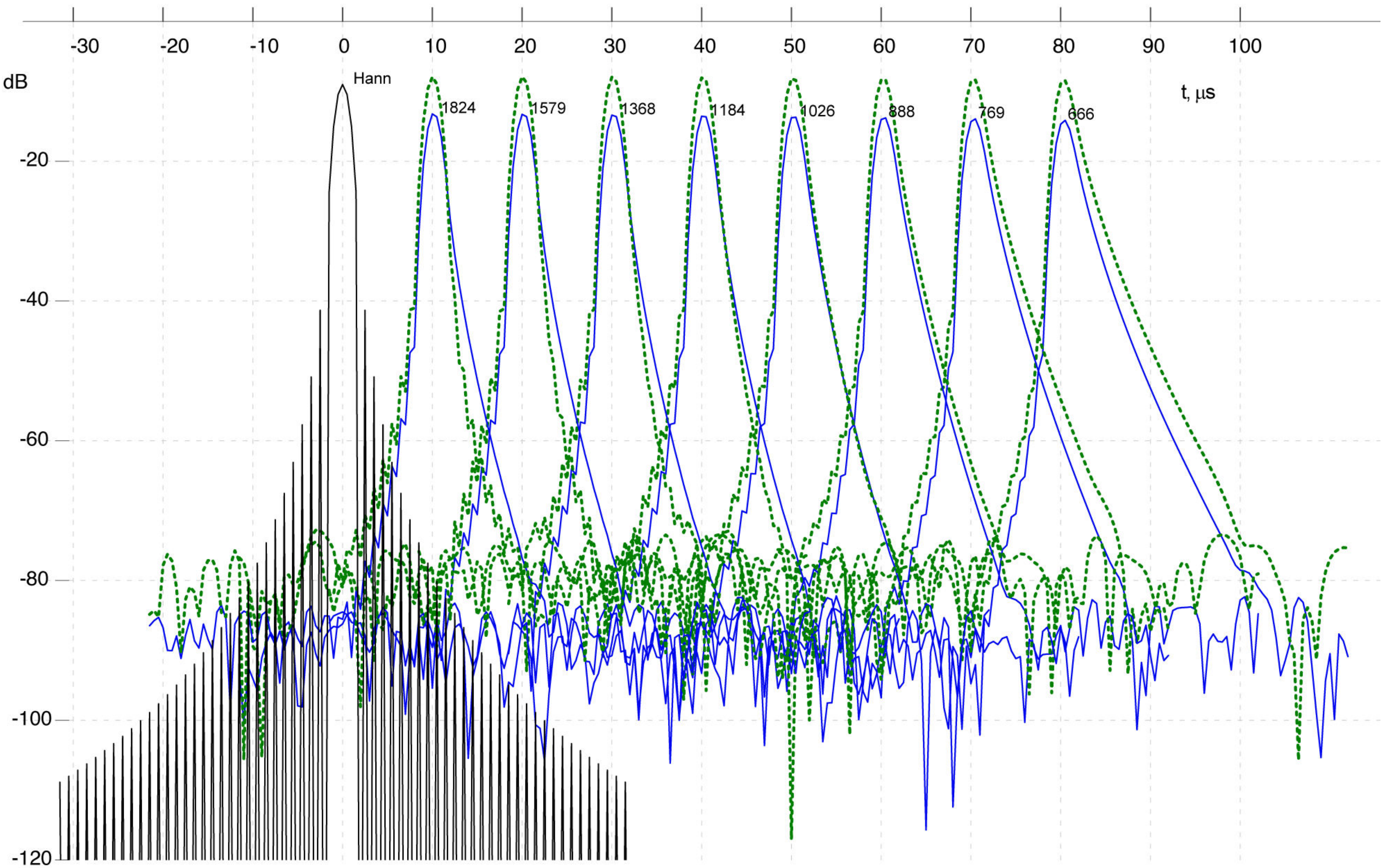

Samples of the simulated GPR signals distorted by the anisotropic ionospheric scintillations. MARSIS BandIV (4.5–5.5MHz). Ionospheric layer thickness H = 15 km, ionospheric plasma frequency fp0 = 4MHz. Plasma density fluctuations level ΔN/N=0.4%

Anisotropic ionospheric fluctuations: degradation and broadening of compressed UWB LFM signals

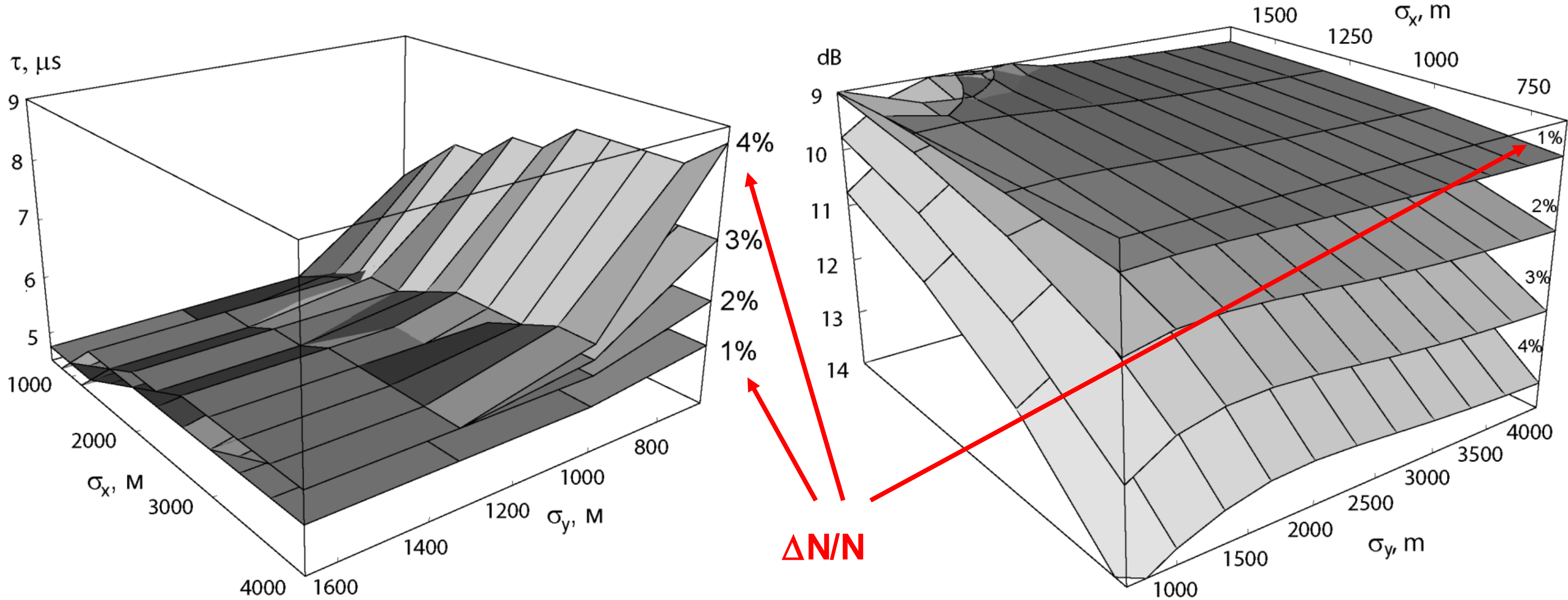

Broadening of the compressed UWB LFM signals' peaks

Degradation of the amplitude of the compressed UWB LFM signals

Non-stationary ionospheric fluctuations (scintillations)

$$B_\varepsilon(\vec{r}_1, \vec{r}_2) =< \varepsilon_1(\vec{r}_1, \omega_1)\varepsilon_1(\vec{r}_2, \omega_2) >$$

$$= \frac{\omega_{p1}^4/(\omega_1\omega_2)^2}{(1-\omega_{p0}^2/\omega_1^2)(1-\omega_{p0}^2/\omega_2^2)} \exp(-\frac{(x_1-x_2)^2}{\sigma_x^2} - \frac{(y_1-y_2)^2}{\sigma_y^2} - \frac{(z_1-z_2)^2}{\sigma_z^2} - \frac{(t_1-t_2)^2}{\tau^2})$$

$$B_\varepsilon(\vec{\rho}, z) \approx A_{\omega_1,\omega_2}(\vec{\rho})\delta z,$$

$$A_{\omega_1,\omega_2}(\vec{\rho}) = \int_{-\infty}^{+\infty} B_\varepsilon(\vec{\rho}, z)dz = A_{\omega_1,\omega_2}(0) \exp(-\frac{(x_1-x_2)^2}{\sigma_x^2} - \frac{(y_1-y_2)^2}{\sigma_y^2} - \frac{(t_1-t_2)^2}{\tau^2})$$

$$A_{\omega_1,\omega_2}(0) = \frac{\omega_{p1}^4/(\omega_1\omega_2)^2}{(1-\omega_{p0}^2/\omega_1^2)(1-\omega_{p0}^2/\omega_2^2)} \sqrt{\pi}\sigma_z$$

Non-stationary fluctuations

Non-stationary ionospheric fluctuations: Gaussian integrals matrices

$$
A_{ij}^{(x)} = \begin{pmatrix}
\frac{n_{12}+n_{13}+n_{14}}{\sigma_x{}^2} - \frac{ik_1(z_1+2z_2)}{4z_1z_2} & \frac{ik_1}{4z_2} - \frac{n_{12}}{\sigma_x{}^2} & -\frac{n_{13}}{\sigma_x{}^2} & -\frac{n_{14}}{\sigma_x{}^2} & \frac{ik_1}{2z_1} & 0 \\
\frac{ik_1}{4z_2} - \frac{n_{12}}{\sigma_x{}^2} & \frac{n_{12}+n_{23}+n_{24}}{\sigma_x{}^2} - \frac{ik_1(z_1+2z_2)}{4z_1z_2} & -\frac{n_{23}}{\sigma_x{}^2} & -\frac{n_{24}}{\sigma_x{}^2} & \frac{ik_1}{2z_1} & 0 \\
-\frac{n_{13}}{\sigma_x{}^2} & -\frac{n_{23}}{\sigma_x{}^2} & \frac{n_{13}+n_{23}+n_{34}}{\sigma_x{}^2} + \frac{ik_2(z_1+2z_2)}{4z_1z_2} & -\frac{ik_2}{4z_2} - \frac{n_{34}}{\sigma_x{}^2} & 0 & -\frac{ik_2}{2z_1} \\
-\frac{n_{14}}{\sigma_x{}^2} & -\frac{n_{24}}{\sigma_x{}^2} & -\frac{ik_2}{4z_2} - \frac{n_{34}}{\sigma_x{}^2} & \frac{n_{14}+n_{24}+n_{34}}{\sigma_x^2} + \frac{ik_2(z_1+2z_2)}{4z_1z_2} & 0 & -\frac{ik_2}{2z_1} \\
\frac{ik_1}{2z_1} & \frac{ik_1}{2z_1} & 0 & 0 & \frac{1}{L^2} - \frac{ik_1}{z_1} + \frac{n_{13}+n_{14}}{\tau^2 v^2} + \frac{n_{23}+n_{24}}{\tau^2 v^2} & -\frac{n_{13}+n_{14}}{\tau^2 v^2} - \frac{n_{23}+n_{24}}{\tau^2 v^2} \\
0 & 0 & -\frac{ik_2}{2z_1} & -\frac{ik_2}{2z_1} & -\frac{n_{13}+n_{14}}{\tau^2 v^2} - \frac{n_{23}+n_{24}}{\tau^2 v^2} & \frac{ik_2}{z_1} + \frac{1}{L^2} + \frac{n_{13}+n_{14}}{\tau^2 v^2} + \frac{n_{23}+n_{24}}{\tau^2 v^2}
\end{pmatrix}
$$

Additional terms due to non-stationary effects

Degradation of the compressed LFM UWB signals due to non-stationary ionospheric scintillations

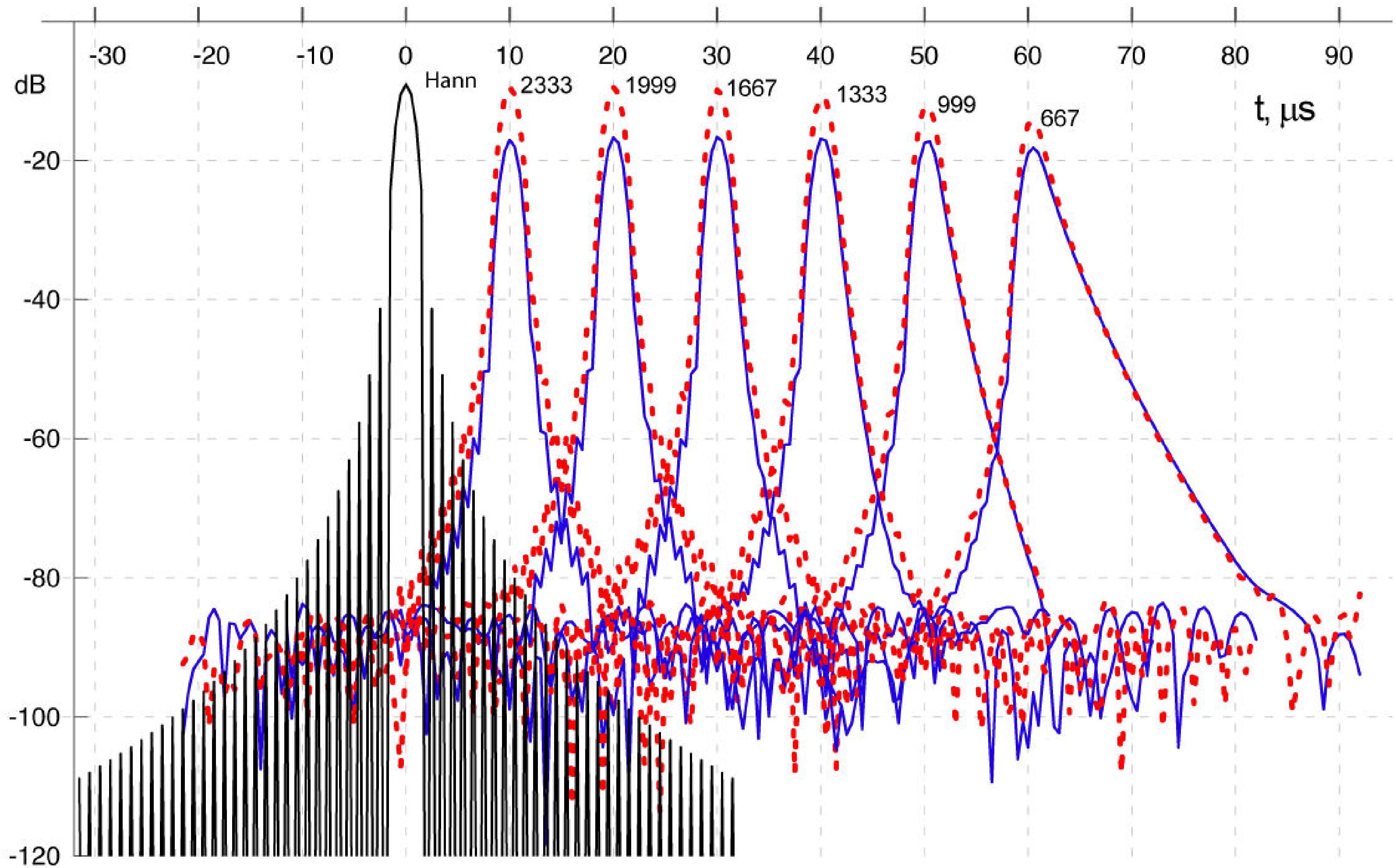

Samples of the simulated GPR signals distorted by the ionospheric scintillations. MARSIS BandIV (4.5–5.5MHz). Ionospheric layer thickness H = 15 km, ionospheric plasma frequency fp0 = 4MHz. Plasma density fluctuations level ΔN/N=0.4%

Non-stationary ionospheric scintillations: degradation and broadening of compressed LFM signals

Correlation function of the plasma inhomogeneities is assumed to be isotropic ($\sigma_x = \sigma_y = \sigma$). Fluctuation levels $\Delta N/N$ are marked by green labels.
The peak amplitude is affected both by σ and Lc while only σ is responsible for the peak broadening.

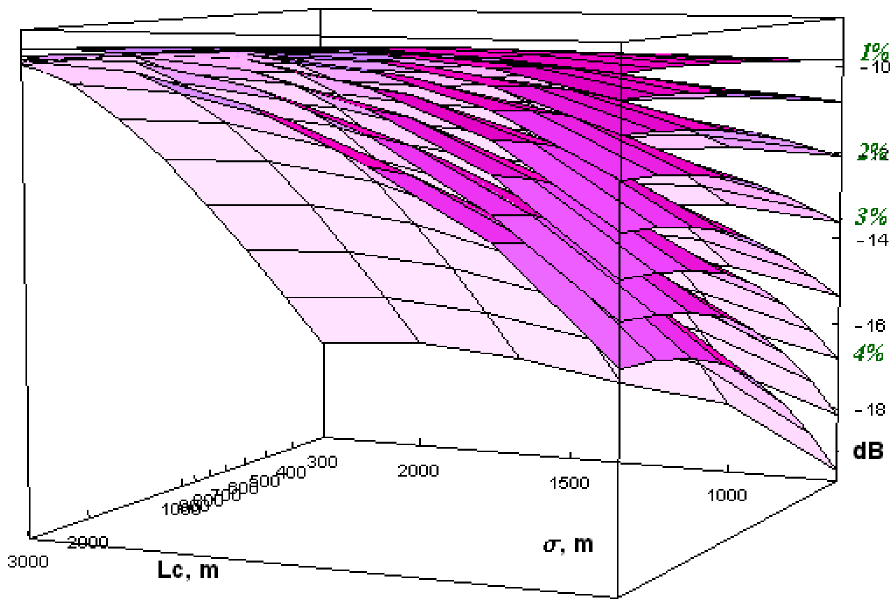

Peak amplitude degradation

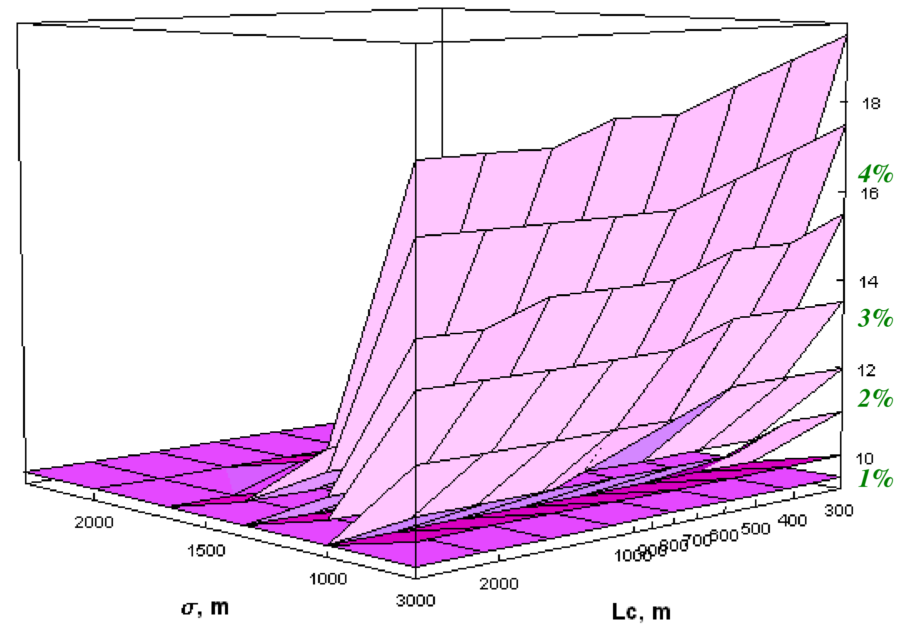

Pulse broadening at ~-50 dB (correction for the amplitude degradation is applied)

$L_c = \tau\, v$ - non-stationary correlation length (distance traveled by the spacecraft during the characteristic period of the scintillations)

Quasi-deterministic phase screen model of the stochastic ionospheric fluctuations

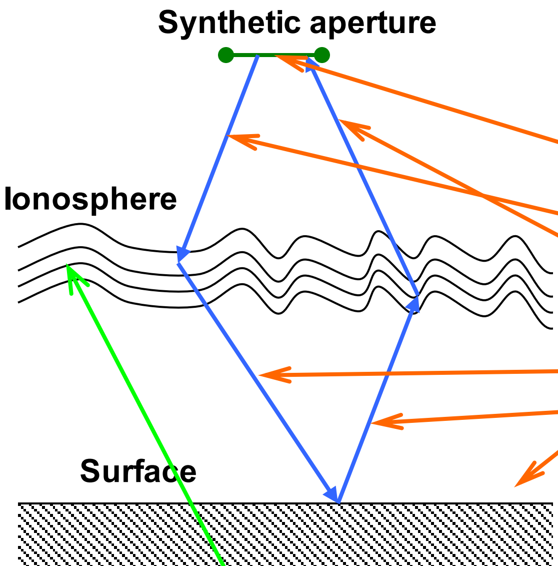

Received field

$$E(\omega) = R(\omega) \int dx_2 dy_2 \int dx_3 dy_3 \int dx_1 \frac{1}{z_1}\frac{k}{4\pi i z_2}\frac{k}{2\pi i z_1}\frac{1}{\sqrt{\pi}L}$$

$$\exp\left(2ikz_1 + i\frac{k(x_1-x_2)^2}{2z_1} + i\frac{k(y_1-y_2)^2}{2z_1} + i\phi(x_2,y_2) + i\frac{k(x_2-x_3)^2}{4z_2} + i\frac{k(y_2-y_3)^2}{4z_2} + i\phi(x_3,y_3) + 2ikz_2 + i\frac{k(x_3-x_1)^2}{2z_1} + i\frac{k(y_3-y_1)^2}{2z_1} - \frac{(x_1-x_0)^2}{L^2} + \frac{i\pi\nu(x_1-x_0)}{L}\right),$$

Field propagation back from the spacecraft to the surface and back to the satellite is described within the paraxial (Kirchoff) approximation

Aperture synthesis is approximately simulated by the integration with Gaussian weight function

Ionospheric phase shift

Numerical simulations

We restrict our attention to the simple quasi-deterministic model of the ionospheric stochastic phase fluctuations, which is essentially 1D superposition of several sinusoidal components with phases and amplitudes

$$\phi(x) = \sum_i A_i \cos(k_i x)$$

It can be shown that the following expansion of the phase shift is valid:

Das Bild kann zurzeit nicht angezeigt werden.

$$\exp(A_1\cos(k_1 x) + A_2\cos(k_2 x) + A_3\cos(k_3 x) + \ldots) =$$
$$= \sum\nolimits_{n_1,n_2,n_3,\ldots} i^{n_1+n_2+n_3+\ldots} J_{n_1}(A_1)\times J_{n_2}(A_2)\times J_{n_3}(A_3)\times\ldots\times\exp(ik_1n_1x + ik_2n_2x + ik_3n_3x + \ldots)$$

where $J_n(\cdot)$ are the cylindrical Bessel functions of the first kind. Substituting this expansion into the integral expression for the registered field, one gets the representation for this field in the form of the discrete sum, which can be easily evaluated with the computer:

$$E(\omega) = R(\omega)\int dx_2dy_2\int dx_3dy_3\,\frac{1}{z_1}\frac{k}{4\pi iz_2}\frac{k}{2\pi iz_1}\sum\nolimits_{n_1,n_2,n_3,m_1,m_2,m_3} i^{n_1+n_2+n_3+m_1+m_2+m_3} J_{n_1}(A_1)J_{n_2}(A_{n_2})J_{n_3}(A_3)J_{m_1}(A_1)J_{m_2}(A_2)J_{m_3}(A_3)$$

$$\exp(ikz_1 + i\frac{k(x-x_2)^2}{2z_1} + i\frac{ky_2^2}{2z_1} + ikz_2x_2 + 2ikz_2 + i\frac{k(x_2-x_3)^2}{4z_2} + i\frac{k(y_2-y_3)^2}{4z_2} + ik_3x_3 + ikz_1 + i\frac{k(x_3-x)^2}{2z_1} + i\frac{ky_3^2}{2z_1})$$

Obtaining of the registered field thus reduces to the evaluation of terms such that

$$\int \exp(-A_{ij}x_i x_j + B_i x_i)d^n x = \sqrt{\frac{\pi^n}{\det A_{ij}}}\exp(\frac{B^T A_{ij}^{-1} B}{4})$$

Variables of integration are separated into two groups (x- and y-), for which the matrix A_i and the vector B_i respectively are

$$A_{ij}^{(x)} = \begin{vmatrix} \frac{1}{L^2} - \frac{ik}{z_1} & \frac{ik}{2z_1} & \frac{ik}{2z_1} \\ \frac{ik}{2z_1} & -\frac{ik(z_1+2z_2)}{4z_1z_2} & \frac{ik}{4z_1} \\ \frac{ik}{2z_1} & \frac{ik}{4z_1} & -\frac{ik(z_1+2z_2)}{4z_1z_2} \end{vmatrix} \quad B_i^{(x)} = \begin{vmatrix} -\frac{iL\pi\nu + 2x_0}{L^2} \\ ik_2 \\ ik_3 \end{vmatrix} \quad A_{ij}^{(y)} = \begin{vmatrix} -\frac{ik(z_1+2z_2)}{4z_1z_2} & \frac{ik}{4z_2} \\ \frac{ik}{4z_2} & -\frac{ik(z_1+2z_2)}{4z_1z_2} \end{vmatrix}$$

$$B_i^{(y)} = 0$$

We omit the intermediate calculations and reproduce the final result:

$$E(\omega) = \sum i^{(n_1+n_2+n_3+m_1+m_2+m_3)} J_{n_1}(A_1)J_{n_2}(A_2)J_{n_{31}}(A_3)J_{m_1}(A_1)J_{m_2}(A_2)J_{m_3}(A_3)$$

$$\exp(-\frac{iz_1((z_1+2z_2)(k_2^2+k_3^2)+2k_3k_2z_1)L^2 + k((k_2+k_3)L^2+\pi\nu L - 2ix_0)^2(z_1+z_2)}{4kL^2(z_1+z_2)})$$

where summation is performed over all six indices $n_1, n_2, n_3, m_1, m_2, m_3$

Dependence on the synthetic aperture length.

Strong phase fluctuations $<\phi^2>=25$

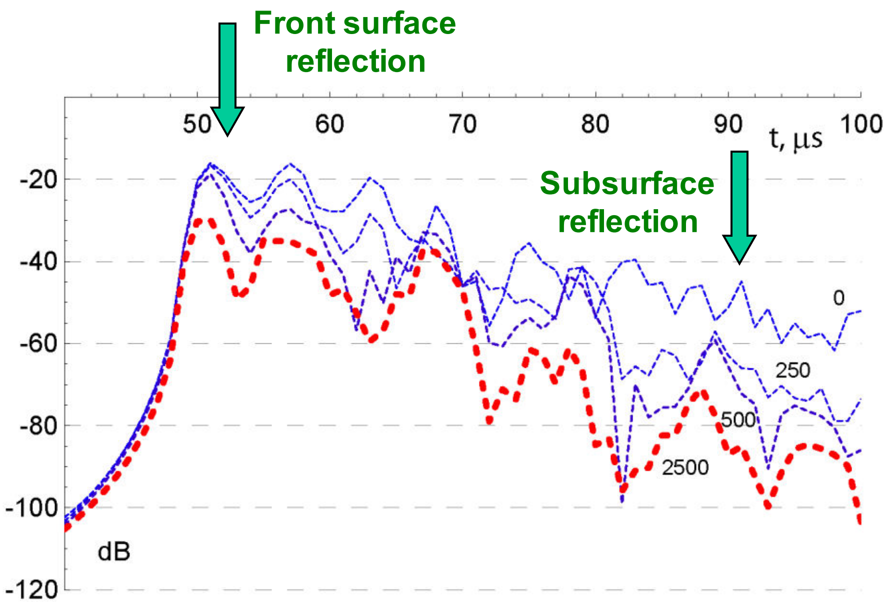

Moderate phase fluctuations $<\phi^2>=4$

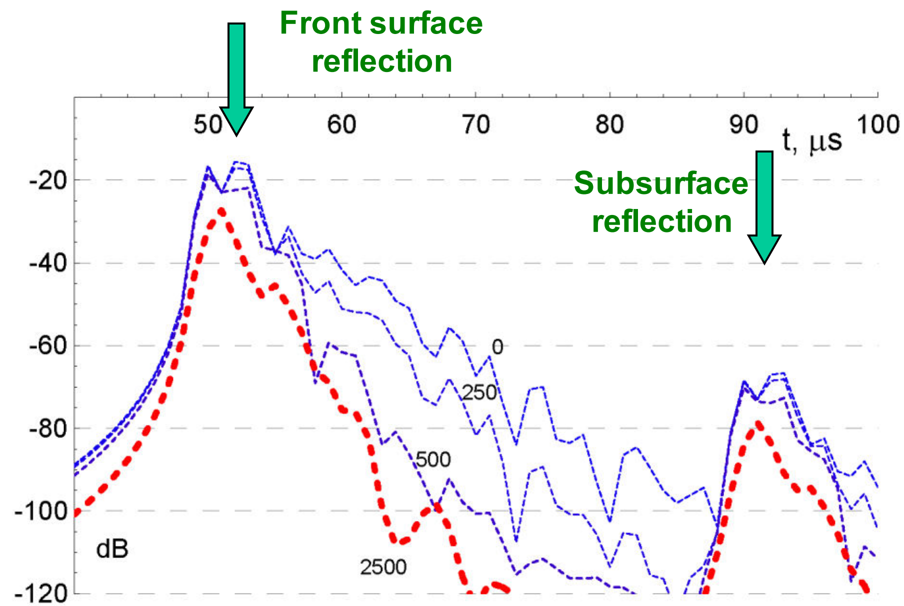

The compressed UWB LFM signals with various synthetic aperture lengths, reflected from the multi-layered subsurface structure, are shown in the figures. The longer the synthetic aperture, the better is the suppression of diffracted peaks in the signals. Extension of the synthetic aperture over the optimal length (half the Fresnel zone size at the central frequency of the LFM band) does not lead to further growth of the suppression.

Aperture synthesis vs. no aperture synthesis

Single pulse (no aperture synthesis)

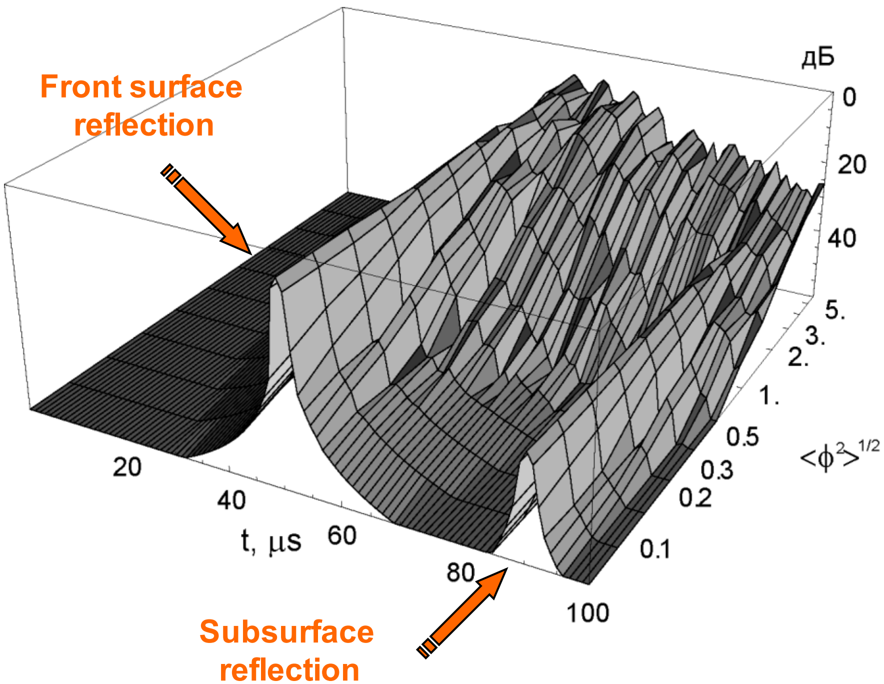

Aperture synthesis (optimal aperture length)

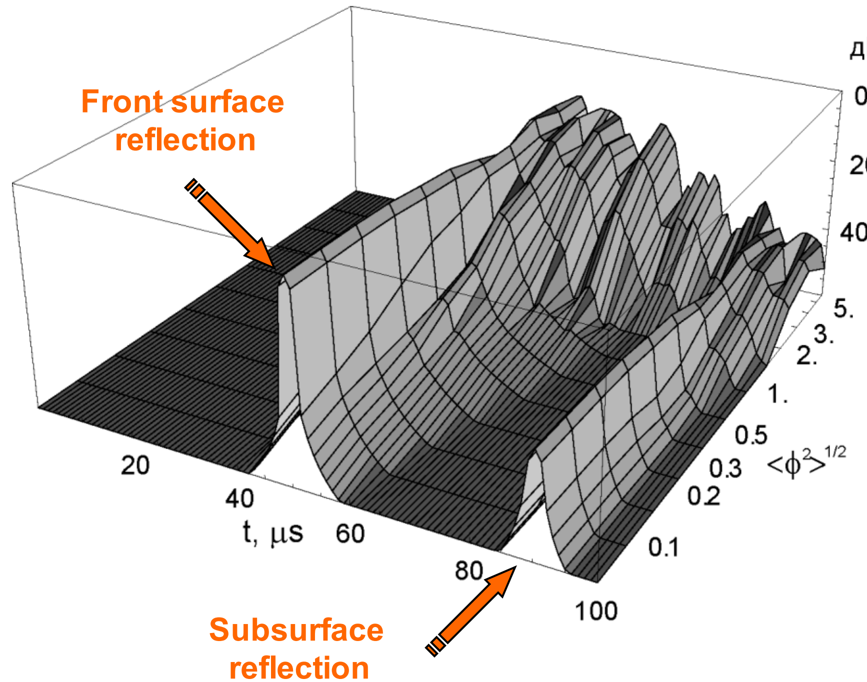

When stochastic phase fluctuations in the ionosphere are of moderate strength (r.m.s. phase deviation does not exceed one whole period), synthetic aperture technique allows to effectively suppress diffracted signals coming from side directions. When the phase fluctuations are stronger than 2π r.m.s., the effect of the aperture synthesis rapidly vanishes.

Subsurface radargram profile: numerical simulation.

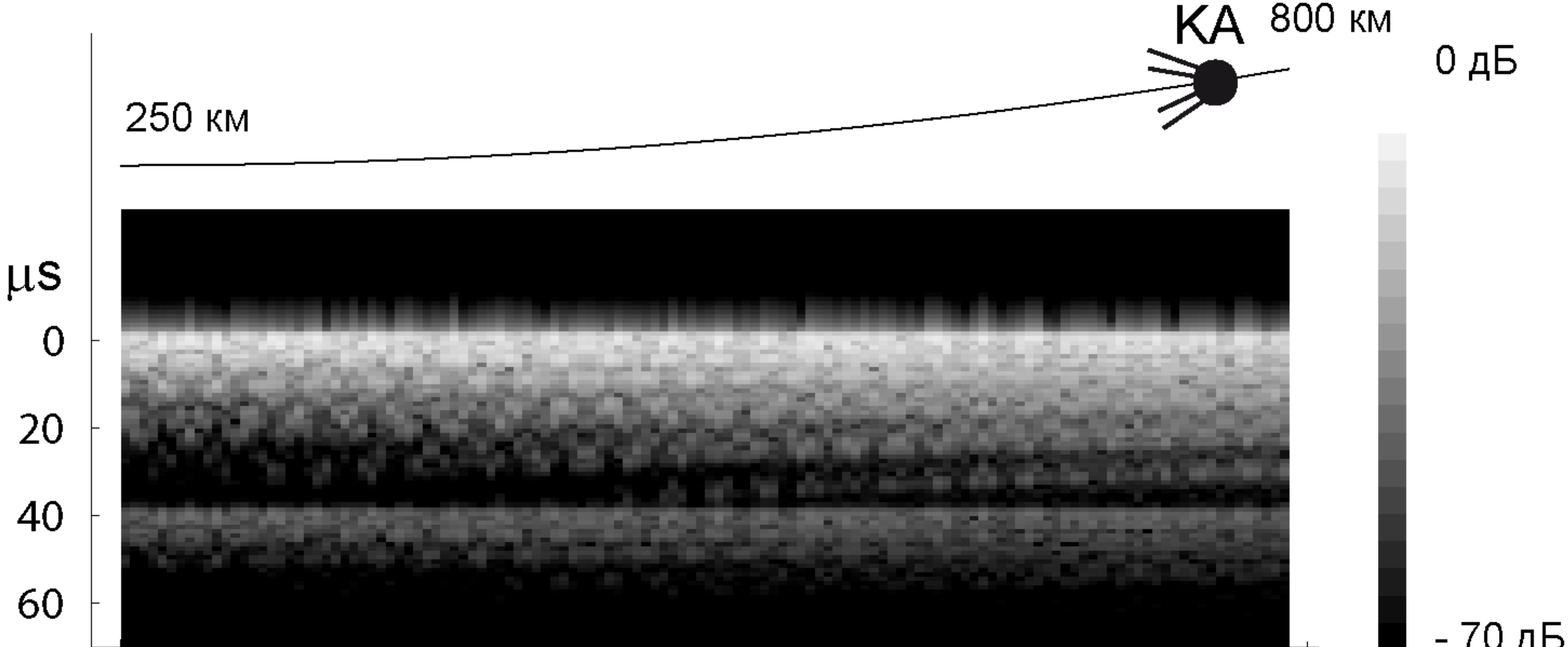

Three schemes of radar sounding of the Martian polar layered deposits

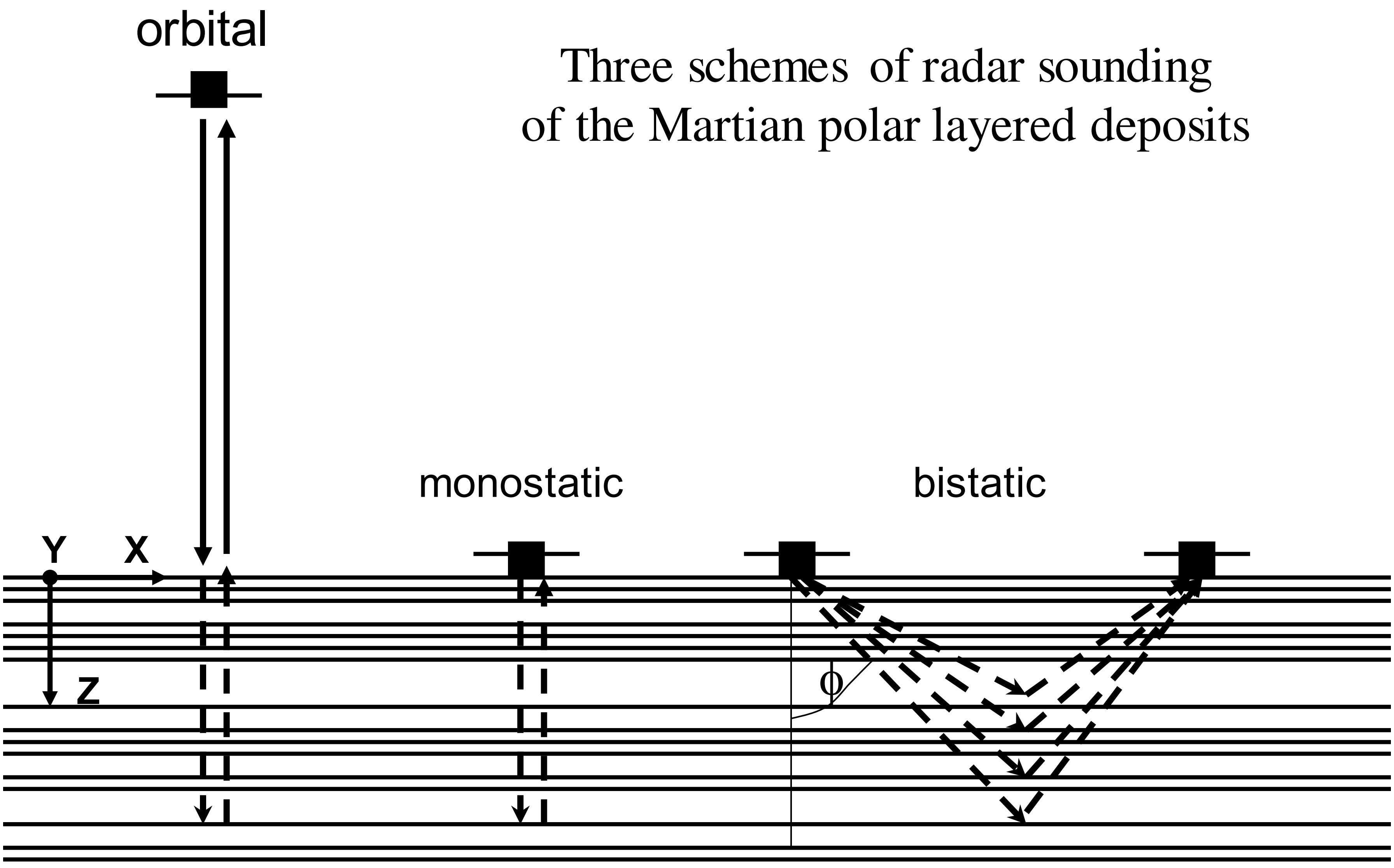

Bistatic radar sounding of the northern polar ice sheet with the landed instrument. 2D model, LFM chirp band 2.5-3.5 MHz TE mode

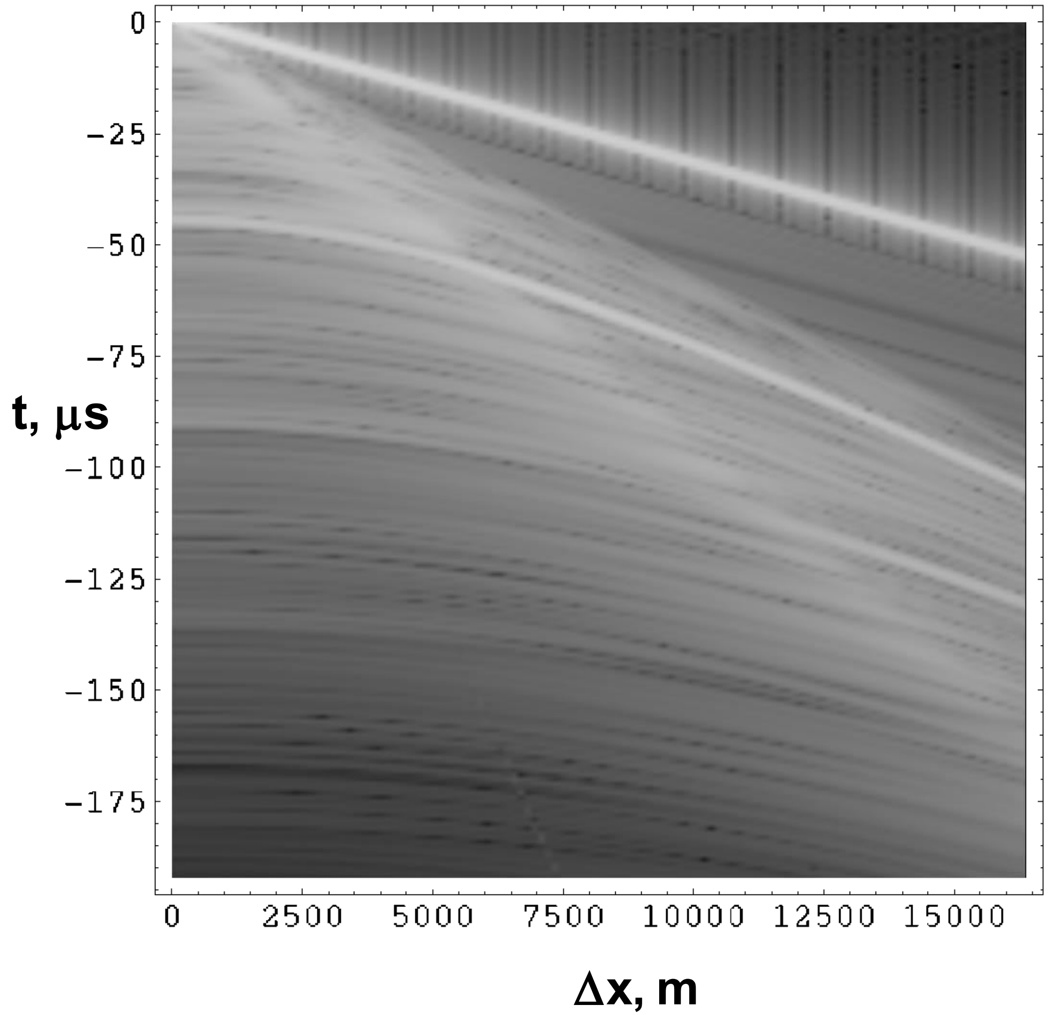

2D geometry

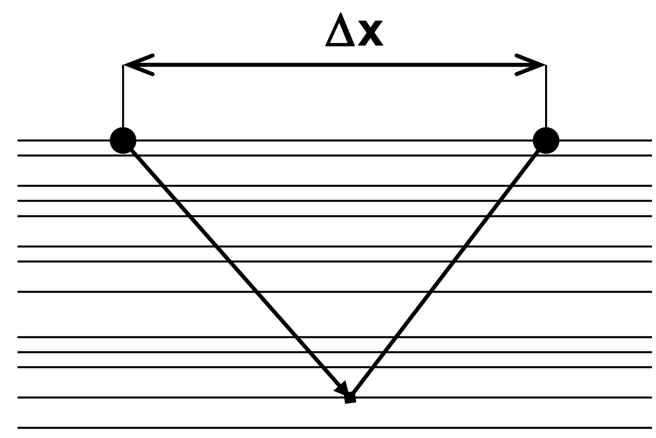

Schematic view of the experiment

Surface and leaky waves:TE and TM mode

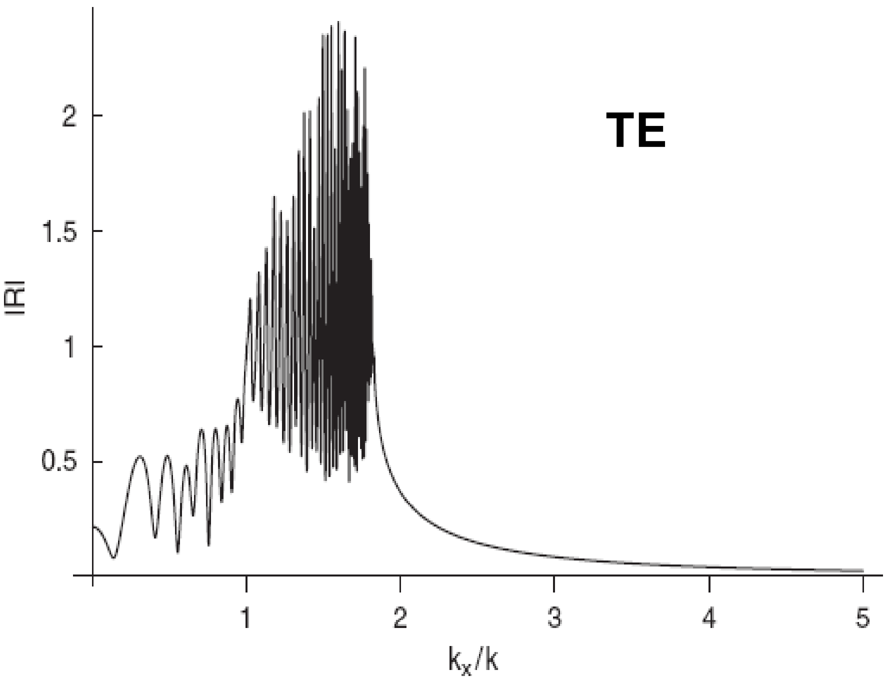

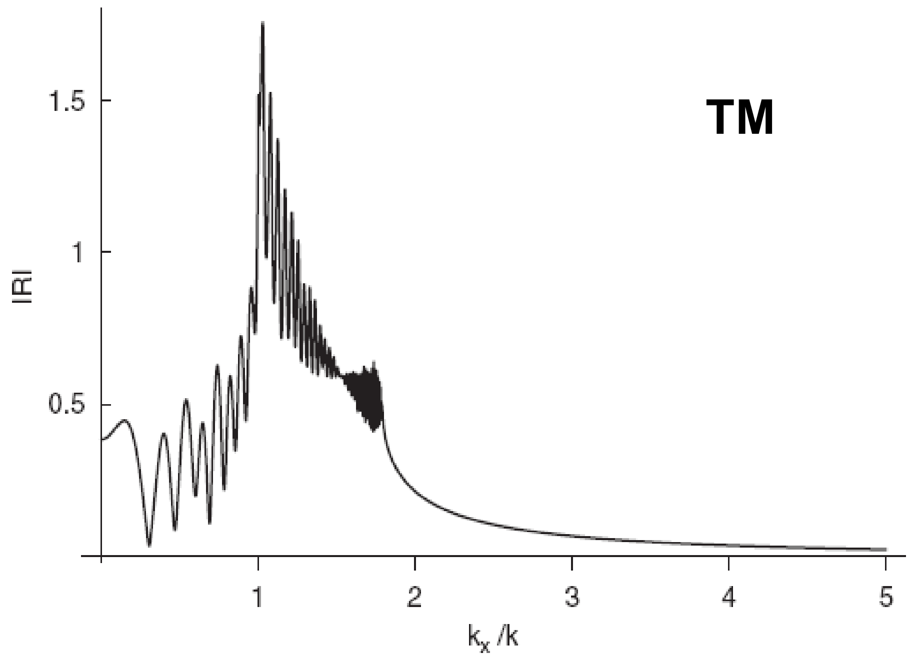

Bistatic radar sounding of the northern polar ice sheet with the landed instrument. 2D model, LFM chirp band 10-15 MHz both TE and TM modes

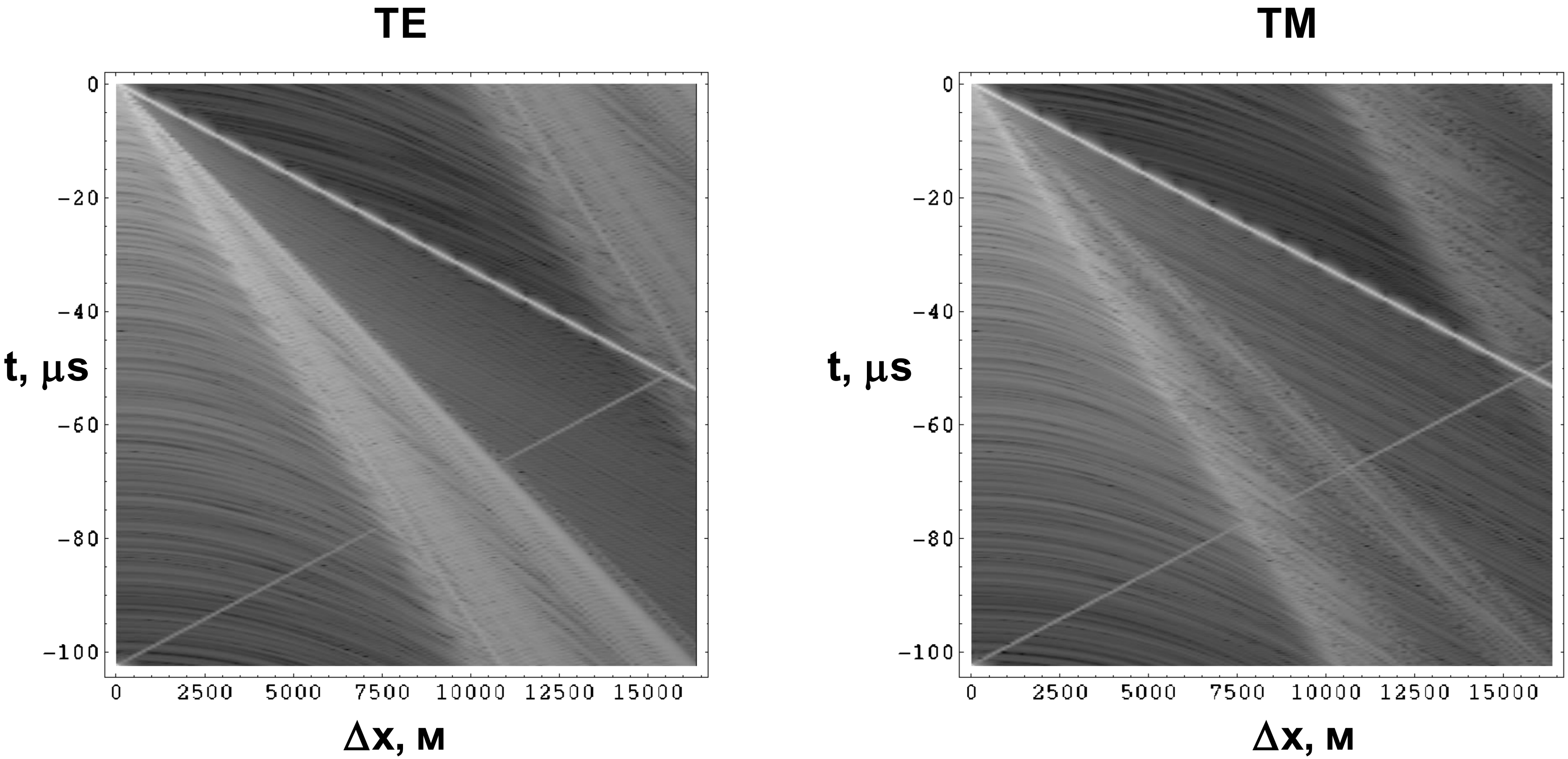

Transverse magnetic (TM) mode demonstrates low reflections at large incidence angles, in particular, close to the Brewster angle.
Dusty layers refractive index n=2.4

Bistatic radar sounding of the northern polar ice sheet with the landed instrument.
3D model, LFM chirp band 10-15 MHz

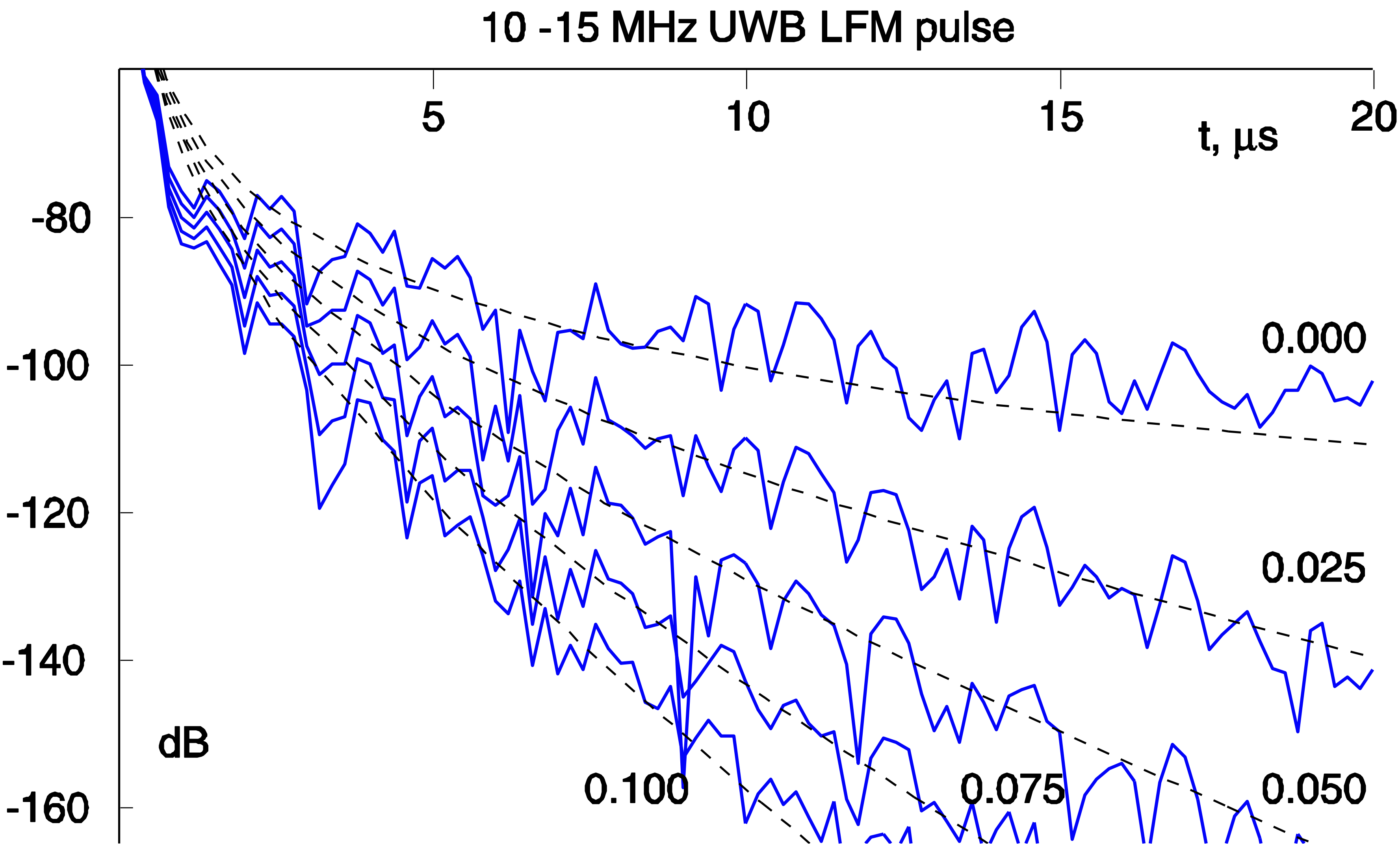

Signal level calibration is arbitrary.
Loss tangents of the dusty layers are shown by numeric labels.

Conclusions and remarks

•The impact of the stochastic small-scale irregular structure of the ionosphere on the performance of the orbital ground-penetrating synthetic aperture radar (SAR) instrument is considered.

•Several numerical models for the computer simulations of the orbital ground-penetrating SAR experiment have been implemented, tested and exploited.

•Different effects, caused by the plasma irregularities and surface roughness, have been revealed and estimated numerically.

•Applicability of the results to the GPR sounding data validation and to the experimental radar studies of the ionospheric irregularities has been discussed.

Thank you for your attention!

Any questions ??